



• Article •
SPECIAL TOPIC:

Multiplexed Survey Telescope: Perspectives for Large-Scale Structure Cosmology in the Era of Stage-V Spectroscopic Survey

Cheng Zhao^{*1}, Song Huang^{†1}, Mengfan He^{1,2}, Paulo Montero-Camacho³, Yu Liu¹, Pablo Renard¹, Yunyi Tang¹, Aurélien Verdier⁴, Wenshuo Xu¹, Xiaorui Yang¹, Jiayi Yu⁴, Yao Zhang¹, Siyi Zhao¹, Xingchen Zhou^{5,6}, Sheng-Yu He⁴, Jean-Paul Kneib⁴, Jiayi Li⁷, Zhuoyang Li¹, Wen-Ting Wang^{8,9}, Zhong-Zhi Xianyu¹⁰, Yidian Zhang⁷, Rafaela Gsponer⁴, Xiao-Dong Li¹¹, Antoine Rocher⁴, Siwei Zou¹², Ting Tan¹³, Zhiqi Huang¹¹, Zhuoxiao Wang¹, Pei Li¹, Maxime Rombach⁴, Chenxing Dong³, Daniel Forero-Sánchez⁴, Huanyuan Shan², Tao Wang^{14,15}, Yin Li³, Zhongxu Zhai^{8,9}, Yuting Wang^{5,16}, Gong-Bo Zhao^{5,17,16,12}, Yong Shi^{14,15}, Shude Mao¹, Lei Huang¹, Liquan Guo¹, and Zheng Cai¹

¹Department of Astronomy, Tsinghua University, Beijing 100084, China;

²Shanghai Astronomical Observatory, Chinese Academy of Sciences, 80 Nandan Road, Shanghai 200030, China;

³Pengcheng Laboratory, Nanshan District, Shenzhen, Guangdong 518000, China;

⁴Institute of Physics, Laboratory of Astrophysics, École Polytechnique Fédérale de Lausanne (EPFL), Observatoire de Sauverny, CH-1290 Versoix, Switzerland;

⁵National Astronomical Observatories, CAS, Beijing 100101, China;

⁶Science Center for China Space Station Telescope, National Astronomical Observatories, Chinese Academy of Science, 20A Datun Road, Beijing 100101, China;

⁷Zhili College, Tsinghua University, Beijing 100084, China;

⁸Department of Astronomy, Shanghai Jiao Tong University, Shanghai 200240, China;

⁹Shanghai Key Laboratory for Particle Physics and Cosmology, Shanghai 200240, China;

¹⁰Department of Physics, Tsinghua University, Beijing 100084, China;

¹¹School of Physics and Astronomy, Sun Yat-sen University, Zhuhai 519082, China;

¹²Chinese Academy of Sciences South America Center for Astronomy (CASSACA), National Astronomical Observatories of China, Beijing 100101, China;

¹³IRFU, CEA, Université Paris-Saclay, F-91191 Gif-sur-Yvette, France;

¹⁴School of Astronomy and Space Science, Nanjing University, 163 Xianlin Avenue, Nanjing 210023, China;

¹⁵Key Laboratory of Modern Astronomy and Astrophysics, Nanjing University, Ministry of Education, 163 Xianlin Avenue, Nanjing 210023, China;

¹⁶Institute for Frontiers in Astronomy and Astrophysics, Beijing Normal University, Beijing 102206, China;

¹⁷School of Astronomy and Space Science, University of Chinese Academy of Sciences, Beijing 100049, China

Received January 11, 2023; accepted April 6, 2023

arXiv:2411.07970v2 [astro-ph.CO] 13 Nov 2024

The MULTiplexed Survey Telescope (MUST) is a 6.5-meter telescope under development. Dedicated to highly-multiplexed, wide-field spectroscopic surveys, MUST observes over 20,000 targets simultaneously using 6.2-mm pitch positioning robots within a $\sim 5 \text{ deg}^2$ field of view. MUST aims to carry out the first Stage-V spectroscopic survey in the 2030s to map the 3D Universe with over 100 million galaxies and quasars, spanning from the nearby Universe to redshift $z \sim 5.5$, corresponding to around 1 billion years after the Big Bang. To cover this extensive redshift range, we present an initial conceptual target selection algorithm for different types of galaxies, from local bright galaxies, luminous red galaxies, and emission line galaxies to high-redshift ($2 < z < 5.5$) Lyman-break galaxies. Using Fisher forecasts, we demonstrate that MUST can address fundamental questions in cosmology, including the nature of dark energy, test of gravity theories, and investigations into primordial physics. This is the first paper in the series of science white papers for MUST, with subsequent developments focusing on additional scientific cases such as galaxy and quasar evolution, Milky Way physics, and dynamic phenomena in the time-domain Universe.

Optical instruments, Sky surveys, Cosmology

PACS number(s): 07.60.-j, 95.80.+p, 98.80.-k

Citation: Zhao, et al.,
 , Sci. China-Phys. Mech. Astron. **66**, 000000 (2023), <https://doi.org/??>

Contents

1	Introduction	000000-3
2	MULTiplexed Survey Telescope	000000-5
2.1	A 6.5-m Telescope for Spectroscopic Surveys	000000-5
2.2	Multiplexed Focal Plane & Instruments	000000-5
2.3	Site and Observing Conditions	000000-7
2.4	Survey Capability and Overall Scientific Potential	000000-7
3	Scientific Motivations of the Stage-V Cosmological Surveys	000000-8
3.1	Nature & Evolution of Dark Energy	000000-8
3.2	Growth of Structure & Nature of Gravity	000000-11
3.3	Inflation & Primordial Physics	000000-12
3.4	Neutrinos & Light Relics	000000-12
3.5	Dark Matter	000000-13
3.6	Synergy with Other Probes	000000-14
3.6.1	Imaging surveys	000000-14
3.6.2	CMB S4	000000-14
3.6.3	Radio surveys	000000-14
3.6.4	Gravitational waves and Fast Radio Bursts	000000-15

*Email: czhao@tsinghua.edu.cn

†Email: shuang@tsinghua.edu.cn

4 Target Selection	000000-15
4.1 Challenges of Target Selection for Stage-V Spectroscopic Surveys	000000-15
4.2 Low-Redshift Tracers	000000-18
4.2.1 Bright Galaxy Sample (BGS)	000000-18
4.2.2 Luminous Red Galaxies (LRG)	000000-18
4.2.3 Emission Line Galaxies (ELG)	000000-19
4.3 High-Redshift Tracers	000000-20
4.3.1 Lyman-Break Galaxies (LBG)	000000-20
4.3.2 Lyman- α Emitters (LAE)	000000-22
4.3.3 Quasi-Stellar Objects (QSO)	000000-22
4.4 Summary of the Targets Selection	000000-22
4.5 Conceptual Survey Design	000000-23
4.5.1 Dark Time Survey	000000-23
4.5.2 Grey Time Survey	000000-23
5 Cosmological Forecasts	000000-24
5.1 Methodology	000000-24
5.2 Dark Energy	000000-25
5.3 Structure Growth & Gravity	000000-25
5.4 Primordial Non-Gaussianity	000000-27
5.5 Neutrinos	000000-27
5.6 Warm Dark Matter	000000-28
6 Conclusions	000000-28

1 Introduction

Over the past four decades, beginning with the “Stick Man” from the CfA Redshift Survey in 1982 [1, 2], spectroscopic mapping of large-scale structures (LSS) has accumulated more than 30 million redshifts of nearby and distant galaxies (see Figure 2). This monumental achievement has contributed significantly to the establishment of the current cosmological model Λ CDM, along with other cosmological probes, i.e., cosmic microwave background (CMB; [3, 4]), Type-Ia supernovae [5-7], or measurements of weak lensing (e.g., [8, 9]). For two decades (2000–2020), major experiments such as the Sloan Digital Sky Survey (SDSS; [10]), followed by the ongoing (2021–2026) survey from the Dark Energy Spectroscopic Instrument¹⁾ (DESI; [11]), have mapped the 3D universe at low and intermediate redshift ($z \lesssim 3$). Clustering measurements from spectroscopic surveys of galaxies and quasars have become a key probe of cosmology. They provide precise measurements on the baryon acoustic oscillations (BAO) scale [12] and the linear growth rate of structure $f\sigma_8$ through redshift space distortions (RSD) [13].

Recent results from the DESI collaboration [14] suggest a potential deviation from the cosmological constant to time-varying dark energy. By the end of this decade, we expect to have sub-percent-level constraints on dark energy and gravity from galaxy clustering up to redshift $z \sim 2$. When the DESI project wraps up, we have finished the spectroscopic survey component of the four stages envisioned by the Dark Energy Task Force (DETF) report [15]. Yet, many fundamental questions remain unanswered, calling for a new era of cosmological experiments in the 2030s.

Going one step further, 3D maps of the universe at high redshift ($z > 2$) will enable the observation of linear modes in the primordial universe, significantly enhancing our ability to constrain dark energy and inflation [16]. In the next decade, a series of ground- and space-based photometric surveys CSST [17], Euclid [18], Nancy Grace Roman Space Telescope [19], LSST [20] will provide deep and high-quality images for future galaxy spectroscopic surveys allowing to target galaxies such as Lyman Break Galaxy (LBG) or Lyman- α emitter (LAE) [21, 22] as tracer of matter at high redshift $2 < z < 5$. Large-volume high-redshift redshift surveys using these new

1) <https://www.desi.lbl.gov/the-desi-survey/>

tracers have the unprecedented potential to help us test primordial non-Gaussianity, probe dynamic dark energy, and reveal possible new features in the primordial power spectrum, uncovering tantalizing hints for new physics.

At the same time, a high-density spectroscopic survey of low-redshift ($z < 1.5$) can provide a high-fidelity 3D map of the cosmic web and trace the matter distributions into the non-linear regimes, opening doors to unexplored scientific opportunities. Such a multi-purpose dataset can also enhance the scientific performance of other cosmological probes, such as calibrating the photometric redshift and intrinsic alignment models for weak gravitational lensing surveys (e.g., [23]; [24, 25]), providing spectroscopic follow-up and host galaxy properties for supernova surveys (e.g., [26, 27]), or exploring new approaches to map the low-redshift large-scale structures (LSS) such as a peculiar velocities survey (e.g., [28, 29]). More importantly, it will help maximize the potential for synergies between spectroscopic surveys and other cosmological probes, such as CMB (e.g., [30]), weak lensing (e.g., [31-34]), and intensity mapping (IM, e.g., [35]) experiments.

Motivated by these two promising directions, the cosmological & high-energy physics community has recently coined the concept for a Stage-V spectroscopic experiment (e.g., [36, 37]) to fulfill these high expectations. By definition, a Stage-V spectroscopic facility should utilize a telescope with high etendue value ($A\Omega$; A and Ω are the collecting area and the field-of-view of the telescope) to ensure a high survey speed. More importantly, the facility should have significantly improved multiplexed capability (number of targets that can be observed simultaneously) compared to the Stage-IV survey (e.g., 5,000 fibers for DESI). Conceptually, a Stage-V facility demands a minimum of 10,000 fibers that could be easily reconfigured to target different objects. This is the primary technical challenge now for such an ambitious vision. At the same time, a Stage-V facility should also have excellent optical performance, high-performance multi-object spectrographs that at least cover the whole optical wavelength range, and a site with good observing conditions. Building on these requirements, multiple ground-based concepts have been proposed, including the 6.5 m MegaMapper telescope [38, 39], the dual-6 m & dual-hemisphere Spec-S5 project²⁾ [40], the 11 m Maunakea Spectroscopic Explorer³⁾ (MSE; [41]), the 12 m Wide-field Spectroscopic Telescope⁴⁾ (WST; [42]), and the ~12 m Extremely Large Spectroscopic Survey Telescope (ESST; [43]).

The MULTiplexed Survey Telescope⁵⁾ (MUST) is a 6.5-

meter telescope [44] under active development. MUST will be located at the 4358 m Peak A of Saishiteng Mountain in Qinghai, China. Equipped with over 20,000 fibers over a $\sim 5 \text{ deg}^2$ field of view (FoV), it features three-channel spectrographs covering wavelengths from 370-960 nm, with spectral resolution between $R = 2,000$ and 4,500. MUST is designed to conduct an ambitious Stage-V cosmological spectroscopic survey, aiming to precisely measure key cosmological parameters and improve our understanding of dark energy and cosmic evolution. With the first light scheduled for 2031, MUST expect to conduct the first Stage-V spectroscopic survey, targeting Lyman Break Galaxy (LBG) and Lyman- α emitter (LAE) at high redshift across $\sim 13,000 \text{ deg}^2$ of the northern sky. Clustering analysis of these tracers will provide sub-percent precision measurements on BAO parameters – $D_A(z)/r_d$ and $H(z)r_d$ – and the linear growth rate of structure, $f\sigma_8$, at redshift $2 < z < 5$, a region not yet covered by current spectroscopic galaxy surveys. Additionally, MUST will provide stringent constraints on primordial non-Gaussianities (PNG, local type) through the parameter $f_{\text{NL}}^{\text{local}}$ with a precision of $\sigma(f_{\text{NL}}^{\text{local}}) \sim 1$. This will enable stringent testing of a wide range of inflationary models. MUST is expected to provide sufficient precision ($\sim 0.03 \text{ eV}$ when combined with CMB data) on the sum of neutrino masses to constrain a nonzero neutrino mass with $\sim 2\sigma$ significance, assuming normal hierarchy. The inverted mass hierarchy can be tested with a significance $\sim 1.3\sigma$. Finally, from power spectrum measurements of the Lyman- α forest, MUST will yield the most precise constraint on warm dark matter mass to date $m_\chi > 10.5 \text{ keV}$ at 95% confidence level (assuming $14,000 \text{ deg}^2$ and $k_{\text{max}} = 0.67 \text{ h Mpc}^{-1}$).

Besides the unique potential of the MUST project, synergies with other cosmological surveys, i.e., future imaging surveys (e.g. CSST, Euclid, LSST), CMB experiments (e.g., Simon Observatory [45], CMB-S4 [46], LiteBird [47]) or radio surveys (e.g., SKAO [48]) will enhance the constraining power of MUST and will result in a better understanding of our Universe. As a dedicated spectroscopic survey facility, MUST can also carry out spectroscopic surveys supporting a wide range of scientific topics outside of LSS cosmology, such as the study of galaxy evolution, super-massive black hole (SMBH), the structure of the Milky Way, and time-domain astrophysics.

This paper describes the MUST instrument and the scientific objectives of the cosmological survey that will be conducted over 5 years of observation. Section 2 provides an overview of the MUST project, including the current status of

2) <https://www.spec-s5.org/>

3) <https://mse.cft.hawaii.edu/>

4) <https://www.wstlescope.com/>

5) <https://must.astro.tsinghua.edu.cn/en>

the whole project, the design of the telescope (Section 2.1), the focal plane system & the spectrograph (Section 2.2), the site & observing condition (Section 2.3), and the overall scientific capabilities (Section 2.4). Section 3 describes the key scientific motivations of MUST for the Stage-V cosmological surveys. The primary scientific goals are covered in detail while briefly summarizing the potential for new probes and the potential synergies with other cosmological surveys. Section 4 presents the current target selection strategy and provides the redshift distribution and target density estimations for the cosmological forecast. We will also introduce the conceptual survey design for MUST. Finally, Section 5 describes the method to forecast the cosmological potential of MUST theoretically and summarizes the forecasted results on dark energy, structure growth, primordial non-Gaussianity, neutrino mass, and warm dark matter constraints. Discussions and main conclusions of this project and future directions are described in Section 6.

Throughout this work, we adopt as fiducial baseline Λ CDM cosmology with parameters $H_0 = 67.6 \text{ km s}^{-1} \text{ Mpc}^{-1}$, $\Omega_b = 0.046$ and $\Omega_m = 0.31$. All magnitudes in this work are defined in the AB magnitude system [49].

2 Multiplexed Survey Telescope

The Multiplexed Survey Telescope (MUST) is a dedicated spectroscopic survey facility proposed and led by the Department of Astronomy at Tsinghua University and co-founded with École Polytechnique Fédérale de Lausanne (EPFL).

The MUST project aims to build a 6.5-meter wide-field telescope with multiplexed spectroscopic observation capability by 2030. While being designed as a flexible platform for various spectroscopic surveys, the primary scientific drive of MUST is to become the first Stage-V spectroscopic survey [50] to answer fundamental questions in cosmology and physics. The concept and early design of MUST drew inspiration from the MegaMapper project [38, 39]. Now, the MUST collaboration has independently finished the preliminary design of the optical system [44], structure, and dome [51] of the telescope and is working with collaborators and vendors to design the modular focal plane, fiber, and spectrograph systems [52]. Here, we briefly introduce the design and the technical capabilities of MUST. A summary of the key specifications is available in Table 1. An upcoming paper will summarize a more detailed description and analysis of the MUST project's technical aspects.

2.1 A 6.5-m Telescope for Spectroscopic Surveys

Driven by the demanding scientific requirements of the next-generation surveys for cosmology, a Stage-V spectroscopic telescope requires excellent optical quality over a large Field-of-View (FoV) on a >6-meter telescope. The optical design of MUST is driven by solving these technical challenges. Currently, MUST adopts a compact Ritchey-Chretien (R-C) design with a multi-element Wide Field Corrector (WFC). The hyperboloid primary and secondary mirrors of MUST are 6.5 m and 2.4 m in diameter. The primary mirror has a 2 m diameter central hole to facilitate the installation of a five-lens WFC that ensures excellent imaging quality of MUST. The largest lens for the WFC of MUST is 1.6 m in diameter, even slightly larger than the largest lens of the camera of LSST [20]. MUST published the conceptual optical design in 2023 [44]. Since then, the collaboration has made a series of modifications, primarily to the configuration of the WFC, to improve the engineering feasibility of the telescope and reduce the risk during the manufacture and assembly of critical sub-systems (Zhang et al. in prep.). Under the updated design, MUST imaging quality over the entire 2.8° diameter FoV is excellent: up to a 50° zenith angle and within the wavelength range of 0.365 to $1.0 \mu\text{m}$, the 80% Encircled Energy (EE80) size of the image spot is $< 0.6 \text{ arcsec}$. At the Cassegrain focus that hosts the modular focal plane system of MUST, the optical system has an F/3.7 focal ratio.

2.2 Multiplexed Focal Plane & Instruments

Enabled by the optimized optical design, MUST can achieve a much more improved multiplexed capability than Stage-IV spectroscopic facilities of today using a novel modular focal plane design (See Figure 1). Starting from the LAMOST survey, modern spectroscopic surveys have adopted different types of robotic fiber positioners ([53-57]) to guide the light from distant targets to the scientific instruments and enable efficient & flexible survey design. The largest multiplexed survey facility, DESI, currently hosts 5,000 fiber positioners, each with a 10 mm outer diameter [58]. Each positioner was installed and operated individually and independently on the focal plate of DESI. However, as a Stage-V facility MUST have a much more demanding requirement for multiplexed capability, individually managing $>10,000$ fiber positioners significantly increases the complexity and the risk of operating the instruments. The MUST collaboration is working with industrial partners to develop a novel modular focal plane system ([59]). As shown in the bottom-right panel of Figure 1, a 1.2 m diameter focal plate will host 336 triangular fiber positioner modules at the Cassegrain focus under the current preliminary design. Each module will integrate 63 fiber positioning robots in three groups.

MUST plans to adopt a miniaturized fiber positioning

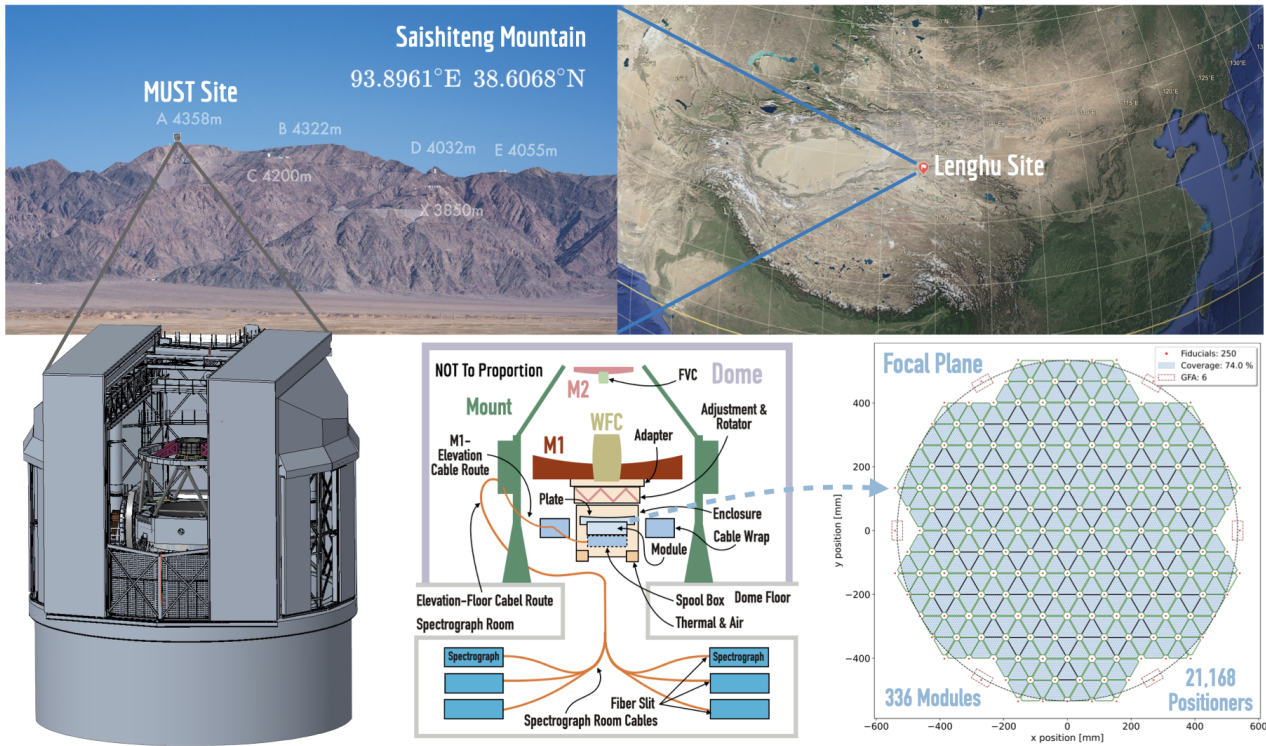


Figure 1 Overview of the MUST project. The top right panel shows the location of the MUST site currently selected in Qinghai province of China. The top left panel is a picture of the Saishiteng mountain near Lenghu. We highlight the peaks that have been or are being developed for astronomy. The highest peak – Peak A – with an altitude of 4358 m, was selected as the site for MUST. From left to right, the bottom panels illustrate the preliminary design of the dome of MUST and the telescope, a sketch of the conceptual design of the focal plane of MUST, fiber, and spectrograph systems, and the fiducial design of the modular focal plane of MUST. By current design, MUST will host 21,168 robotic fiber positioners using 336 triangular modules.

Optical System			
Optical Design	R-C with WFC		
Primary Mirror Diameter	6.5 m Hyperboloid	With 2 m central hole	
Secondary Mirror Diameter	2.4 m Hyperboloid	Convex	
Wide Field Corrector	Five-Lens Design	Largest lens diameter: 1.6 m	
Throughput Requirement	> 50% from 370-960 nm	Considering the reflectance of the primary & secondary mirror, WFC throughput, and the vignetting of the secondary & corrector	
Focal Ratio	F/3.7	Cassegrain Focus	
Field of View	2.8° in Diameter		
Focal Plane & Fiber System (Preliminary)			
Focal Plane Diameter	1.2 m		
Total # of Modules	336	Semi-frameless design	
# of Positioners per Module	63	21 × 3 groups	
Total # of Fiber Positioners	21,168		
Effective Positioner Coverage	74.0%		
Pitch Distance between Positioners	6.2 mm	Using a θ - ϕ design	
Fiber Core Diameter	150 μ m	1.3 arcsec on the sky	
Fiber Route Length	45-50 m	From the fiber tip to the slithead	
Spectrograph (Preliminary)			
Channel	Wavelength Coverage	Spectral Resolution	Average Throughput
Blue	370-590 nm	R~ 2513-3668	≥ 55%
Red	565-775 nm	R~ 2287-3442	≥ 60%
NIR	750-960 nm	R~ 4124-5279	≥ 60%

Table 1 Summary of the key specification of the optical, focal plane & fiber, and spectrograph systems of MUST. Note that the design specifications for the focal plane and spectrograph systems are still very preliminary.

robot with a 6.2 mm outer diameter and optical fiber with a 150 μm core diameter corresponding to 1.3 arcsecs on the sky to ensure the fiber density satisfies the requirement of future cosmology surveys. To optimize the effective coverage of the fibers, the focal plate assembles four modules into a group. The gaps between modules are 1 mm and 3 mm within the group and between adjacent groups. Altogether, this allows MUST to equip 21,168 fiber positioners over the focal plane with a 74% coverage, which results in a $\sim 5 \text{ deg}^2$ FoV covered by fibers with a $\sim 4,000 \text{ deg}^{-2}$ fiber density. It is worth noting that, given the aspheric shape of the focal plane and the requirements of the fiber throughput & focal ratio degradation (FRD) budgets of MUST, the fiber tips of all the positioners should be located within $\pm 50 \mu\text{m}$ from the theoretical focal plane. The design of MUST achieves this goal by approximating the focal plane with a best-fit spherical surface that meets the requirement. In this way, all the modules can have an identical configuration, and within each module, the tips of the 63 positioners will match the shape of the spherical surface. This challenging and ambitious design is essential to the overall scientific capability of MUST, especially for the LSS survey discussed here.

The first-generation instruments of MUST consist of ~ 42 multi-object spectrographs; each will host ~ 500 optical fibers on a $4\text{k}\times 4\text{k}$ -pixels CCD detector. The preliminary design of the spectrograph of MUST is still underway. Regardless, given the very similar scientific goals to the DESI project, the current concept adopts a similar three-channel design as the spectrograph of DESI, covering the wavelength range between ~ 3700 to $\sim 9600 \text{ \AA}$ with a $R \sim 2000$ to 4000 spectroscopic resolution. We currently aim to achieve a $> 60\%$ average throughput in all three channels while exploring different approaches to further improve it to an average $\sim 70\%$ efficiency.

In addition to the fiber positioning system and the spectrographs, the scientific instrument system of MUST includes other crucial sub-systems, such as the fiber view camera (FVC), fiducial fibers, focal plate adjustment & derotation mechanism, and a complex fiber route (see Figure 1). Altogether, they will enable the Stage-V LSS survey potential of MUST. In the upcoming publications, we will describe the technical design of the whole focal plane system and the spectrographs.

2.3 Site and Observing Conditions

MUST has selected the Peak A of the Saishiteng Mountain near the Lenghu Town in Haixi Mongol and Tibetan Autonomous Prefecture, Qinghai Province, China, as its can-

didate site (referred to as the ‘‘Lenghu’’ site). The Lenghu site was first reported in [60] and has been selected by a series of domestic astronomical projects in China, including the Mozi Survey Telescope⁶⁾ (a 2.5 m wide field imaging survey telescope in operation) and the Jiao-tong University Spectroscopic Telescope (JUST; a planned 4 m segmented mirror telescope; [61]), and more. Along with several other peaks (see Figure 1), Peak A, at 4,358 m, has been flattened for construction. Starting from Oct. 2023, the MUST collaboration has begun to monitor the weather and seeing condition on Peak A. While we are still accumulating data for a more precise site condition assessment, combining our data with the public data collected by the NAOC team at the nearby Peak C⁷⁾, we estimate that the Lenghu site has an annual clear night fraction between 60% to 70%, with worse observing conditions during the summer, and a median DIMM seeing FWHM between 0.8 to 1.0 arcsec. These specifications satisfy the site requirement to carry out a fiber-spectroscopic survey. While the light pollution from the development of nearby towns and mining businesses is a concern, the local government has passed legislation to protect the dark night conditions within a 50 km area around the Lenghu site.

At 4,358 m, Peak A enjoys significantly less atmospheric attenuation in the shorter wavelength range. Preliminary photometric observations from the Mozi telescope point to the promising result that the atmospheric attenuation level at $\lambda < 450 \text{ nm}$ of Lenghu is comparable with that of Mauna Kea and is much better than lower altitude sites such as Kitt Peak. This presents MUST the opportunity to improve the overall throughput in the blue wavelength end, which is crucial for identifying the Lyman- α ($\text{Ly}\alpha$) emission line at $z > 2$. Meanwhile, the high altitude also results in a median nighttime air temperature of -8.1°C (minimum & maximum temperatures are -25°C and 15.2°C), which increases the challenges for the construction and maintenance of MUST. At the same time, the median nighttime humidity is $\sim 30\%$ at Peak A.

2.4 Survey Capability and Overall Scientific Potential

Given the current monthly statistics of clear night fraction, the Lenghu site could provide $\sim 2,400$ and 2,800 observing hours per year. Assuming a configuration with 20,000 working fibers and a $> 90\%$ up time, MUST will have 210-270 million fiber hours in a five-year survey, allowing MUST to conduct Stage-V LSS surveys. As a dedicated survey facility, the long-term commitment of MUST to spectroscopic surveys is another unique strength in fulfilling the Stage-V cosmological goals. Compared to DESI, MUST has a 3.4 \times higher light collecting capability and 4 \times more fibers. Even

6) <https://wfst.ustc.edu.cn/>

7) <http://lenghu.china-vo.org/>

considering the throughput costs of the secondary mirror, the more complex WFC design, the longer fiber route, and challenges in the spectrograph design, MUST can still improve the spectroscopic survey efficiency – the number of redshifts measures for the same set of targets during the same time – by $\sim 10\times$.

While the Stage-V cosmological survey will be the highest priority of MUST during the first phase of its operation, the significant fiber-hour budget will allow us to design versatile programs with a wide range of scientific goals. In addition to mapping the large-scale structures for cosmology, the same dataset will enable robust statistical studies of galaxies and Active Galactic Nuclei (AGN) near and far. These data can help us understand the rise and fall of star formation in galaxies in the last 10 Gyrs and the assembly of different populations of galaxies. It will also enable us to measure the accretion rate and mass of supermassive black holes (SMBHs) in a galaxy sample that is one order of magnitude larger than the existing one and significantly improve our understanding of the growth of SMBH and its impact on galaxy evolution. At the small, non-linear scale, the detailed picture of galaxy clustering will enable better modeling of galaxy-halo connections, which will help cosmology in return. During bright nights, MUST can measure the radial velocities and chemical abundances of many halo stars in the Milky Way to shed light on its assembly history and constrain the nature of dark matter. Located at a longitude less populated with large ground-based telescopes, MUST is also poised to play an exciting role in the age of time-domain spectroscopic surveys. The list can go on.

In addition, the modular focal plane of MUST secures future opportunities for instrument upgrades: high-resolution fiber spectrograph and integrated field spectrograph (IFS) can be straightforwardly added to the focal plane as long as their front-end optics fit into the current fiber positioner module. In the following publications from this series, we will discuss these topics' scientific potential and strategy in detail.

For the rest of this work, we will focus on the first and foremost scientific goal of MUST: the first Stage-V LSS spectroscopic survey to deepen our understanding of several fundamental questions in cosmology and physics.

3 Scientific Motivations of the Stage-V Cosmological Surveys

Ever since the discovery of the accelerated expansion of the Universe using type Ia supernova data [64, 65], Λ CDM has been widely accepted as the standard cosmology model (cf., however, [66], for earlier observational evidence of a nonzero Λ). However, several key components of the Λ CDM

model remain unknown, such as the physical origin of Λ (or, more generally, dark energy), the nature of dark matter, and the establishment of initial conditions of cosmic structures. Meanwhile, several observational challenges to Λ CDM have emerged as the precision of cosmological measurements improves (e.g., [67]). Massive spectroscopic surveys are expected to help address these issues. By analyzing the clustering of large-scale structures (LSS) from spectroscopic data, we can investigate the properties of dark energy and dark matter through the dynamic evolution of the Universe governed by these competing components and extract signatures of fundamental physical processes at extremely high energy scale in the primordial Universe.

In this section, we review the scientific motivations of the next-generation (Stage-V) spectroscopic survey to be carried out by MUST. Figure 3 shows some of the key scientific cases that can be tested by MUST with a high significance level.

3.1 Nature & Evolution of Dark Energy

Dark energy is one of the key scientific problems of our time and poses a significant challenge to the Standard Model of particle physics. While CMB observations suggest that dark energy constitutes about 70% of the energy density of the Universe in the Λ CDM model [4], its physical properties are largely unexplored. One exception is the equation of state (EoS) parameter w , which influences the dynamics of the Universe and can be probed through geometrical measurements. The most straightforward interpretation of dark energy is the cosmological constant (Λ), corresponding to a constant $w = -1$, which is well consistent with most observations to date (e.g., [4, 10]). A natural extension beyond Λ involves introducing dynamic dark energy, which potentially originates from various physical mechanisms [68] and leads to a time-evolving EoS parameter typically expressed as

$$w(a) = w_0 + w_a(1 - a), \quad (1)$$

where w_0 is the current value of w and w_a quantifies its time evolution. For instance, the quintessence model, describing a dynamical scalar field minimally coupled to gravity, typically yields $w \gtrsim -1$, while the phantom energy, a scalar field with negative kinematic energy, predicts $w < -1$. Observational constraints on w_0 and w_a provide a pathway to distinguishing these models.

The constraints on EoS parameters rely primarily on geometrical probes, including “standard(-isable) candles” such as Cepheids and type Ia supernovae (e.g., [7]), and “standard rulers” such as Baryon Acoustic Oscillations (BAO; [69]) and the matter-radiation equality scale (e.g., [70]). BAO arises from acoustic density waves in the primordial Universe and

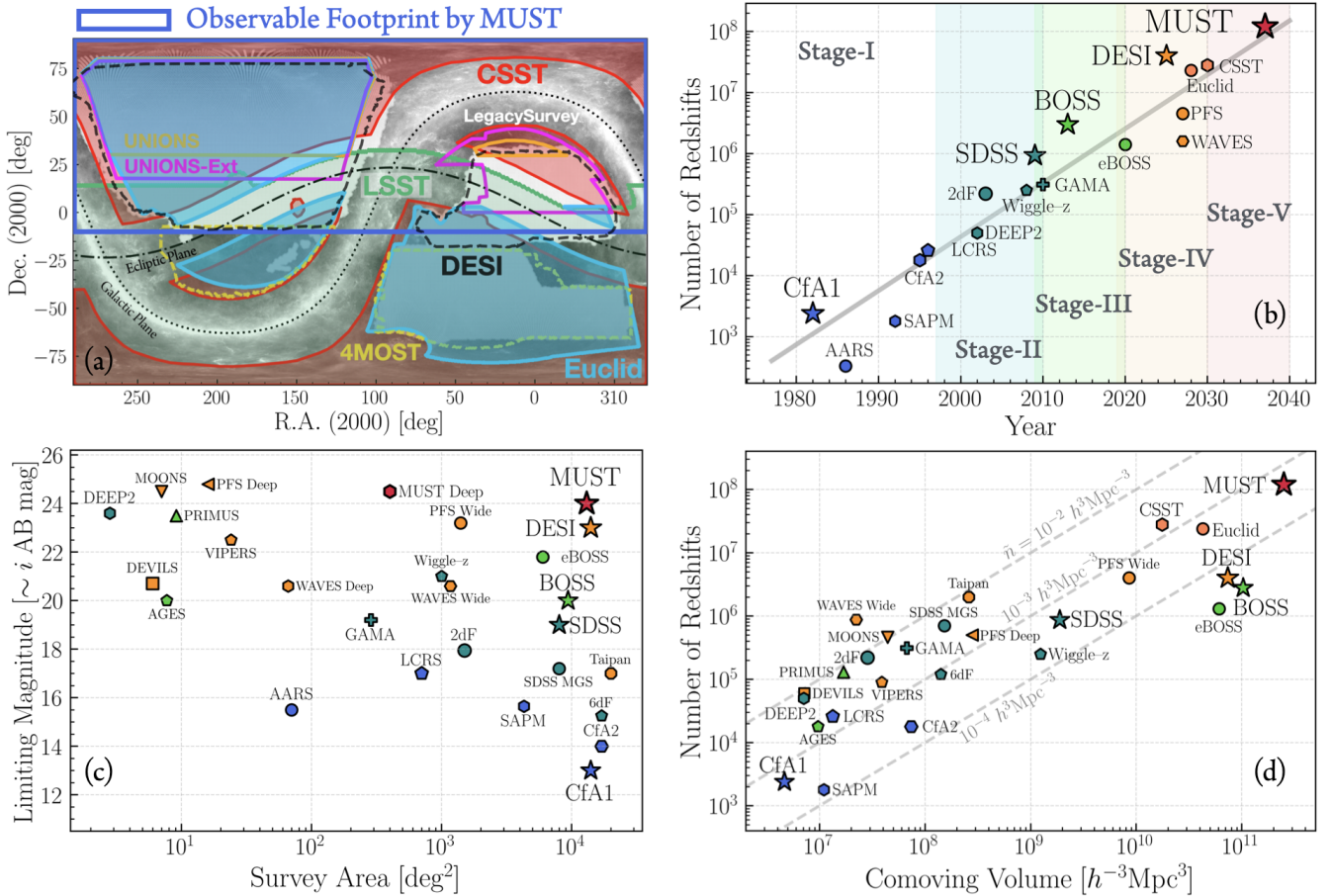


Figure 2 (a) Full sky map displaying relevant imaging (CSST red, UNIONS yellow/purple, LSST green, and Euclid light blue) and spectroscopic (DESI black, 4MOST light yellow) surveys on top of the dust opacity map from the Planck mission [62]. The survey area reachable by MUST is highlighted in blue (dec > -10°). CSST, UNIONS, LSST, and Euclid will be critical for the target selection of the cosmological survey of MUST. (b) Evolution of the number of galaxy redshifts from redshift surveys starting from the CfA1 survey in the early 1980s. The shaded regions with different colors represent the rough separations between various stages of large-scale structure surveys for cosmology. The star symbols highlight a few signature surveys for the previous four stages of spectroscopic surveys. MUST strives to become the first Stage-V (red background) survey in operation in the early 2030s. (c) Apparent magnitude limit in i -band reachable by different redshift surveys as a function of the survey area. (d) Number of redshifts as a function of the comoving volume of redshift galaxy surveys. In the two bottom panels, the colors of the symbols reflect the different cosmology stages. These different metrics highlight the unique scientific potential of MUST.

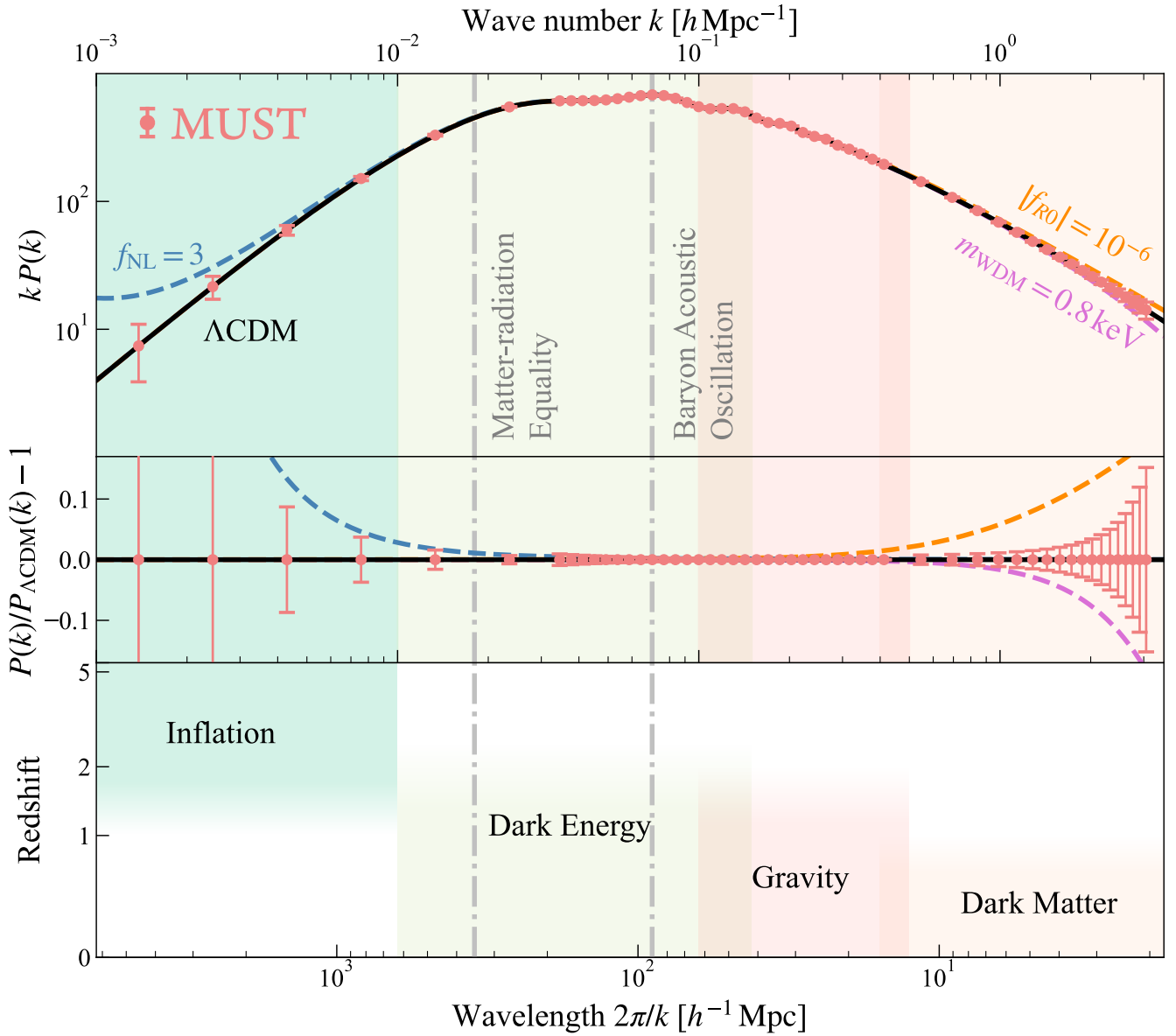


Figure 3 *Top panel:* A schematic diagram illustrating power spectra of various cosmological models, with error bars predicted from the current survey design of MUST. *Middle panel:* A ratio plot highlighting MUST's ability to distinguish between different cosmological models. *Bottom panel:* Key science cases for different scales and redshifts. The fiducial ΛCDM power spectrum is based on Planck 2015 results [63]; error bars and power spectra of different cosmological models are rescaled to the fiducial power spectrum accordingly. Error bars for $k < 0.4 h \text{ Mpc}^{-1}$ are estimated using Eq. (15) with the expected bias and number density of MUST's LBG sample, while those for $k > 0.4 h \text{ Mpc}^{-1}$ are obtained from Ly α 3D power spectrum forecasts, taking into account the effects of spectroscopic systematics and the quasar luminosity function. MUST's unprecedentedly large survey volume enables probing of the large-scale power spectrum with high accuracy, which is crucial for distinguishing between different inflation models. Moreover, MUST's high sample number density allows for precise measurements power spectrum at small scales, which is sensitive to science cases such as dark matter properties and modified gravity models.

produces an excess of matter correlation amplitude at a characteristic comoving scale of $\sim 100 h^{-1}$ Mpc. By extracting the BAO signal from the clustering of matter tracers, such as galaxies and QSOs, we can probe the expansion rate of our Universe and thus constrain dark energy models. Recently, the tomographic Alcock–Paczynski (AP) test, which performs geometrical measurements based on the response of the apparent shape of galaxy clustering to the adopted cosmological model for redshift-to-distance conversion, has also been shown as a complementary probe of dark energy [71].

Observational programs for measuring the dark energy EoS have been strategically planned to proceed through successive stages of cosmic surveys, as outlined in the Dark Energy Task Force report [15]. Since the first detections of the BAO signal from galaxies at $z < 0.47$ [12, 72], subsequent spectroscopic surveys have extended BAO measurements to galaxies across a wide redshift range (up to $z < 1.5$), as well as QSOs and Lyman- α tracers at even higher redshifts [10]. These efforts have substantially improved the precision of w measurements. Recently, DESI, a Stage-IV dark energy survey, reported a w consistent with Λ CDM with an uncertainty of $\sim 2.5\%$ [73]. However, when the EoS is allowed to vary over time, current spectroscopic data hint at the potential dynamical behavior of dark energy (e.g., [74]). With its unprecedented survey efficiency, MUST is expected to deliver even more precise BAO measurements, covering a redshift range from the nearby Universe to $z \sim 5.5$. Thus, MUST meets the requirements of a Stage-V dark energy survey suggested by the Snowmass Cosmic Frontier report [75] and may offer deeper insights into the potential evolution of dark energy (see Section 5.2). Additionally, we will investigate the possibility of improving dark energy constraints using alternative probes, such as the tomographic AP test and the matter-radiation equality scale.

3.2 Growth of Structure & Nature of Gravity

Within the framework of hot Big Bang cosmology, gravity amplifies primordial density perturbations of the order of 10^{-5} seeded by inflation in an expanding cosmic background, leading to the formation and growth of LSS. As a result, the growth of structures is a sensitive probe of both gravity theories and dark energy. Notably, in modified gravity theories that deviate from General Relativity (GR), the intrinsic relationship between structure growth and geometrical quantities is generally altered or even disrupted. Thus, monitoring the structure growth over time provides stringent tests of gravity theories [76].

The growth of cosmic structures largely shapes the spatial correlations and the amplitude of peculiar velocities of galaxies. One prominent effect is redshift-space distortions (RSD;

e.g., [77]), where the observed redshift maps of galaxies are distorted by their peculiar velocities along the line of sight. This distortion leads to the anisotropic clustering of galaxies, which allows for measurements of the autocorrelation of galaxy velocity divergence $P_{\theta\theta}$ and its cross-correlation with galaxy densities $P_{g\theta}$. In this context, the effect of structure growth can be parameterized through the combination of the linear growth rate and the amplitude of matter fluctuations $f\sigma_8$, as the power spectra scale as $P_{\theta\theta} \propto (f\sigma_8)^2$ and $P_{g\theta} \propto f\sigma_8$ (e.g., [78]).

Another common approach to test gravity theories is to compare the two gravitational potentials Ψ and Φ by parameterizing them with phenomenological functions μ and Σ that linearly perturb GR (e.g., [10, 79, 80]). Many modified gravity theories of cosmological interest can be represented using the following equations, which allow the two potentials to differ:

$$k^2\Psi = -4\pi G a^2(1 + \mu(a, k))\rho\delta, \quad (2)$$

$$k^2(\Psi + \Phi) = -8\pi G a^2(1 + \Sigma(a, k))\rho\delta. \quad (3)$$

Here, ρ indicates the background matter density and δ is the comoving density perturbation. The functions μ and Σ effectively describe the variations of matter density field and changes of lensing effect on massless particles, respectively. Comparing measurements of μ and Σ to their fiducial values of zero thus constitutes a test of deviations from GR.

Galaxy spectroscopic surveys enable structure growth measurements through both correlations of galaxy velocities and comparisons of the spatial clustering of galaxies across different redshifts. Testing gravity is, therefore, a primary scientific motivation of recent spectroscopic surveys, such as SDSS and DESI [11, 81]. Currently, measurements of structure growth at $z \lesssim 1$ have achieved precision at the $\lesssim 10\%$ level (e.g., [10], see also Section 5.3). While results from spectroscopic surveys are generally consistent with predictions of the GR- Λ CDM model, the structure growth history at high redshifts remains largely unexplored. Probing this regime is essential for differentiating between various gravity theories. As a Stage-V cosmological survey, MUST is expected to fill in this gap and provide substantial improvements in our understanding of gravity theory, as well as deeper insights into the tension between cosmic shear and matter perturbations from CMB measurements (e.g., [8]).

MUST also has the potential to measure relativistic effects, such as the gravitational redshifts, that are sensitive to gravity theories but have been too subtle to be detected with current data [82]. These effects can introduce additional distortions to galaxy clustering beyond RSD, primarily generating odd Legendre multipoles in the cross-correlation of different galaxy populations that can be measured from galaxy spectroscopic data.

3.3 Inflation & Primordial Physics

Large-scale structures (LSS) of the Universe not only trace the evolution of the Universe but also encode rich information about its initial conditions generated during a primordial era. The most prominent scenario for the primordial universe is cosmic inflation, which refers to a nearly exponential expansion of the universe by roughly 60 e -folds in a blink. To probe the microscopic quantum fluctuations of the spacetime and matter/fields during inflation that created the LSS [83,84] is a primary motivation for MUST.

Through setting the initial conditions of the LSS, inflationary cosmology provides a wealth of observables that reveal the dynamics of the primordial universe and, more interestingly, the fundamental physics at the inflation scale. Current theory and observations suggest that the inflation scale could be up to $O(10^{13} \text{ GeV})$ [85], which is much higher than the energy scale of any imaginable terrestrial experiments. Therefore, primordial fluctuations provide a unique window into high-energy fundamental physics, complementing other high-energy experiments.

The inflation predictions on the primordial scalar power spectrum have been delicately measured at the CMB scale through the overall amplitude A_s and the spectral index n_s [85]. These parameters are also expected to be measured by MUST by extracting the primordial scalar power spectrum from the LSS data. However, due to the near-scale invariance of the scalar fluctuation at large scales, the information extractable from the power spectrum is limited, although there have been ongoing efforts in searching and understanding tiny scale-dependent (and very often oscillatory) features in the power spectrum [86,87]. On the other hand, a vast amount of information can be revealed by going to higher n -point ($n \geq 3$) correlations of scalar modes, which are traditionally known as primordial non-Gaussianity (PNG; [88,89]). There is in principle fruitful information encoded in the PNG, though historically, many efforts have been made to the search of 3-point statistics, such as bispectra $B(k_1, k_2, k_3)$ on a few particular shapes (the bispectrum dependences on the ratios of k_i where $i = 1, 2, 3$), including the local, equilateral, and orthogonal shapes (e.g., [90-93]).

The overall amplitudes of these shapes are parameterized by dimensionless parameters called f_{NL} , which are crucial cosmological parameters for the next generation LSS surveys. Within typical single-field slow-roll inflation models, it is worth noting that the minimal signal of equilateral bispectrum coming from the gravitational interaction of the scalar modes is $f_{\text{NL}} \sim O(10^{-2})$, which, if detected, would mark our detection of gravitational interaction [94]. However, other fundamental interactions, particles, and fields besides the inflaton field may carry stronger-than-gravity coupling to the

scalar mode. Thus, it is possible that more significant signals can be detected, which will revolutionize our understanding of the primordial universe and fundamental physics. Typically, $f_{\text{NL}} \sim 1$ is a crucial threshold for the theories with and without the slow-roll condition [95,96].

There have been active searches of f_{NL} , especially for the local shape ($f_{\text{NL}}^{\text{local}}$), but a firm detection has not been made yet. The state-of-the-art constraint comes from CMB measurements by Planck, with $f_{\text{NL}}^{\text{local}} = -0.9 \pm 5.1$ [97]. Meanwhile, galaxy spectroscopic surveys are becoming more promising as LSS clustering can be very sensitive to the PNG through the scale-dependent galaxy bias [83,98,99]. Current bounds on the local shape bispectrum from spectroscopic surveys are $|f_{\text{NL}}^{\text{local}}| \sim O(20-30)$ (e.g., [91]). MUST, as a Stage-V spectroscopic survey, is expected to improve the constraints on f_{NL} significantly with the benefit of the increasing survey volume and redshift range, surpassing current CMB constraints (see Sec. 5.4).

Besides the traditional ‘‘PNG’’ searches, recent years have witnessed the fast development of new directions, such as cosmological collider (CC) physics. For instance, oscillatory signals of n -point correlation functions can be generated by the resonance between heavy states spontaneously created during inflation and scalar (or tensor) modes and encode a wealth of information about the evolution history of spacetime and the dynamical information of the heavy particle, including the mass, spin, sound speed, chemical potential, interaction type, etc. [100,101] Meanwhile, parity-odd patterns in galaxy clustering have gained considerable attention recently. If confirmed, they will be a clear signal of new physics. Active efforts are ongoing in search for these signals in current data and forecast for detectability from future observations [99,102-104]. To maximize the potential scientific outcome of MUST, we aim to explore the feasibility of achieving these goals with MUST in subsequent studies.

3.4 Neutrinos & Light Relics

The existence of neutrino mass, as revealed by atmospheric and solar neutrino experiments, provides strong evidence for new physics beyond the Standard Model. Neutrino oscillation experiments suggest two possible hierarchies in their mass spectrum: the normal ($m_1 < m_2 < m_3$, $M_\nu \gtrsim 0.059 \text{ eV}$) and the inverted ($m_3 < m_1 < m_2$, $M_\nu \gtrsim 0.099 \text{ eV}$) hierarchies, where m_1 , m_2 , and m_3 indicate the 3 mass eigenstates, and M_ν denotes the total neutrino mass [105]. Determination of the mass hierarchy is essential for understanding the nature of neutrinos (Dirac or Majorana) and formulating the generalized standard model. However, the most stringent constraint on M_ν from current particle physics experiments, set by the KATRIN experiment [106], is only $M_\nu \lesssim 1.4 \text{ eV}$ at the 90 %

credible level (CL). This limit is insufficient to distinguish between the mass hierarchies.

Neutrinos act as radiation in the early Universe and subsequently contribute matter-energy budget at the late Universe with $\Omega_\nu = M_\nu/(93.14 h^2 \text{ eV})$, which alters the expansion rate and shifts the redshift of matter-radiation equality. Besides, due to their significant velocity dispersion, massive neutrinos slow down the growth of structures, resulting in a suppression of the matter power spectrum below the neutrino free-streaming scale [107, 108]. As a result, LSS probes are sensitive to the total neutrino mass, providing complementary constraints to particle physics experiments.

In addition to neutrino mass, the clustering of galaxies also permits constraints on the effective number of neutrino species N_{eff} , which can be used to probe non-standard neutrino interactions [109, 110] or extra light thermal relics from the primordial Universe, such as light sterile neutrinos [111] and axions [112-114]. This is because N_{eff} can be inferred from the phase shift of the BAO spectrum. Any deviation from the value $N_{\text{eff}} = 3.044$, as predicted by the standard cosmological model with 3 massive neutrino species, notably if exceeding 1 %, would indicate new physics beyond the Standard Models of particle physics and cosmology.

It is worth noting that the constraints on M_ν and N_{eff} from CMB alone exhibit a geometrical degeneracy with H_0 (or Ω_m). BAO measurements can help break this degeneracy due to their ability to constrain Ω_m [4, 73]. Combining CMB and LSS data has already led to more stringent constraints on M_ν than those from terrestrial experiments, approaching the lower bound in the inverted hierarchical scenario [115-117]. Recently, DESI reported an upper bound of $M_\nu < 0.072 \text{ eV}$ (95 % CL) with a prior of $M_\nu > 0 \text{ eV}$, and updated the constraint $N_{\text{eff}} = 3.10 \pm 0.17$, which is in remarkable agreement with the Standard Model expectation. With its significantly larger survey volume and increased tracer number density, MUST is expected to substantially tighten constraints on both parameters and investigate the possibility of distinguishing between the two mass hierarchies in combination with data from next-generation CMB experiments (e.g., CMB-S4 [118]).

3.5 Dark Matter

Although dark matter (DM) – which constitutes $\sim 25 \%$ of the energy density of the Universe – was first postulated almost 90 years ago [119], its fundamental nature remains unknown. Observational efforts have focused mainly on the cold dark matter (CDM) paradigm, yet its constituents remain elusive, prompting interest in alternative DM models. These

alternative models aim to address specific challenges to the CDM model, such as the missing satellite, cusp-core (e.g., [120, 121]), and too-big-to-fail problems [122] (see [123] for a review).

Popular alternatives to the CDM model include warm dark matter (WDM; see e.g., [124, 125]), fuzzy dark matter (FDM; [126, 127]), self-interacting dark matter (SIDM; [128, 129]), and primordial black holes (PBH; see e.g., [130, 131]). These models gain traction for their potential to mitigate the challenges of CMB or for their natural origin, such as PBHs, which do not require new physics beyond the standard model. MUST can offer unique insight into discovering the nature of dark matter primarily through two avenues: Milky Way (MW) and Local Group (LG) observations, as well as the Ly α forest.

In the current *Gaia* era, the measurement of dark matter distribution around our MW based on stellar kinematics still has significant uncertainties (e.g., [132]). One dominant reason is model extrapolations due to the lack of stellar tracers with full phase-space information in the outer MW halo ($\gtrsim 100 \text{ kpc}$). MUST can measure the line-of-sight velocities (LOS v) of a plethora of MW halo stars, which, in combination with a deep proper motion survey (e.g., the Roman space telescope high-latitude survey [133]), will allow for the mapping of the local distribution of dark matter (e.g., [134]) around our MW, enabling constraints on the radial mass profile and 3D shape of the MW dark halo, which will significantly benefit direct dark matter detection programs (e.g., [135]).

In particular, the ongoing Stage-IV DESI Milky Way survey (MWS; [136]) reaches $\sim 20 - 30 \%$ completeness for MW targets in the flux range of $16 < r < 19$. MUST can potentially reach fainter magnitudes than DESI and thus can provide more distant MW halo star LOS v s and increase the completeness at similar magnitudes as DESI, bringing in better constraints on the dark matter distribution in the outer halo. In addition to halo stars, dwarf galaxies and stellar streams around our MW and in the LG carry valuable information on the nature of dark matter (e.g., [129, 137-142]), and MUST can potentially measure the LOS v s for member stars in distant dwarf galaxies or streams to better infer their mass content or past interactions with dark matter clumps.

The Ly α forest consists of absorption features in the spectra of distant quasars caused by Lyman- α transitions of neutral hydrogen in the foreground intergalactic medium (IGM). Thus, the Ly α forest is a biased tracer of the neutral hydrogen distribution, and hence, it probes the underlying dark matter density field. As a dark matter probe covering higher redshifts than traditional galaxy surveys, the forest has been used

8) However, the Ly α forest is unlikely to detect subtle differences between dark matter models [143], such as the oscillations predicted by FDM at very

to measure the BAO feature; nonetheless, its relatively high redshift $2 \lesssim z \lesssim 5$ and sensitivity to small-scale clustering ($\gtrsim 1$ Mpc) make it an ideal probe of dark matter models⁸⁾. For instance, constraints from the 1D Ly α flux power spectrum, obtained from medium and high-resolution spectra, set a firm lower limit on the WDM particle mass of $m_\chi \geq 5.3 - 5.7$ keV [145, 146].

Although MW astrophysics and the Ly α forest can provide robust dark matter constraints, the accuracy of these constraints depends on careful modeling of baryonic physics and nonlinearities (e.g., [143]). In particular, Ly α forest constraints require precise modeling of IGM astrophysics [147-150] due to the degeneracies between the response of IGM to cosmic reionization and the impact of non-cold dark matter on the thermal state of the IGM. With a conservative flux limit of $r \leq 23.5$ (larger than that of DESI, which is $r < 23$) and an estimated quasar number density surpassing 80 deg^{-2} at $z > 2.1$, MUST is expected to refine our ability to constrain dark matter models using the Ly α forest (see 5.6 and Figure 10).

3.6 Synergy with Other Probes

3.6.1 Imaging surveys

Next-generation space-based wide-field imaging surveys such as the China Space Station Telescope (CSST; [17]), Euclid [151], and Roman [152] will measure galaxy shears with unprecedented precision, providing tighter dark energy constraints with weak lensing. The ground-based Legacy Survey of Space and Time (LSST; [20]) will observe the whole southern sky every few nights, building the most extensive catalog of transient phenomena of cosmological interest such as type Ia supernovae or variable AGN. Other imaging surveys worth noting are the Hyper Suprime-Cam Subaru Strategic Program (HSC-SSP; [153, 154]) and the Mozi Wide Field Survey Telescope (WFST; [155]), which will provide deeper broad-band sky coverage than currently available data, as well as the Javalambre Physics of the Accelerating Universe Survey (J-PAS; [156]), a narrow-band imaging survey with higher-precision photometric redshifts.

Apart from using imaging data from these surveys for MUST target selection, we aim to maximize the scientific outcome through joint analyses of the data for cosmological measurements or even dedicated coordinated observations. For instance, the spectroscopic and photometric samples can be cross-correlated to break degeneracies associated with intrinsic alignments and galaxy bias, thus improving the precision of cosmological measurements (e.g., [157, 158]). Additionally, spare fibers of MUST can be used to complete the

spectroscopic data of galaxies in color space to expand the training set for the calibration of photometric or slitless spectroscopic redshift measurements (e.g., [31, 159]). The high efficiency and large survey volume of MUST offers opportunities to identify or confirm strong lensing systems, e.g., low- z bright galaxies with anomaly high- z emission lines [160]. Moreover, the cross-correlation between imaging data and Ly α forests from MUST may enable tracing LSS using Ly α intensity mapping [161].

3.6.2 CMB S4

The next generation of CMB experiments, such as AliCPT [162], Simons Observatory [163], CMB-S4 [164], LiteBIRD [165], and PICO [166], holds significant promise for detecting primordial gravitational waves from the early-universe inflationary epoch. Precisely measuring primordial gravitational waves faces two significant obstacles: foreground contamination and gravitational lensing distortions. Consequently, accurate reconstruction of the CMB lensing potential is critical for isolating the primordial signal. Multi-tracer delensing methods, which leverage galaxy survey data, are expected to significantly enhance the capability of CMB experiments to detect the elusive primordial gravitational waves [167].

In addition to enhancing our understanding of inflationary physics, MUST will facilitate synergistic investigations of large-scale structures. This includes the measurement of the kinetic Sunyaev-Zel'dovich (kSZ) effect, which provides insights into the dynamics of baryonic matter (e.g., [168]). Furthermore, cross-correlations with CMB lensing will improve our understanding of structure formation (e.g., [30]). With these complementary approaches, MUST, in combination with next-generation CMB experiments, promises to enrich our understanding of cosmic evolution.

3.6.3 Radio surveys

The Square Kilometre Array (SKA; [48]) will conduct an IM program using the 21 cm hyperfine transition of neutral Hydrogen. Due to the significant disparity in strength between foreground emissions and the cosmological 21 cm signal – differing by several orders of magnitude – confirming the cosmic origin of the signal, particularly at high redshifts ($z \gtrsim 1$), will likely require cross-correlations with other cosmological tracers. Current studies typically focus on cross-correlations with high-redshift galaxies [169, 170], LBG [171], and the Ly α forest [172, 173]. These complementary approaches coupling 21 cm measurements with spectroscopic surveys enhance our ability to discern the cosmological signal from

small scales [144].

foreground contamination, thus improving the robustness of IM measurements.

MUST will significantly enhance cross-correlation efforts involving 21 cm observations with high-redshift galaxies and the Lyman- α forest, enabling measurements with high signal-to-noise. Such cross-correlations will be instrumental in advancing our understanding of various cosmological phenomena, such as dark energy constraints [174], modified gravity [175], dark matter [176], and hydrogen reionization [173].

3.6.4 Gravitational waves and Fast Radio Bursts

Very high-energy, transient phenomena such as gravitational waves and Fast Radio Bursts (FRBs) may also provide valuable cosmological constraints. Ever since the first detection of a gravitational wave event by LIGO [177], several large observatories are projected, e.g., LISA [178], Taiji [179], TianQin [179] and the Einstein Telescope [180]. In addition to the detection of singular events, the gravitational wave background has also been recently detected by Pulsar Timing Array collaborations (e.g., NANOGrav, [181], CPTA [182], EPTA, [183]). Regarding FRBs, current radio observatories detect these events regularly, compiling ever-growing catalogs with hundreds of events (e.g., CHIME, [184], ASKAP, [185], MeerKAT [186], FAST [187]).

The most direct synergy MUST will have is the measurement of redshifts and peculiar velocities for both gravitational waves and FRBs electromagnetic (EM) counterparts. Gravitational waves from binary inspirals act as standard sirens since their luminosity distance can be inferred from their observation [188]. Hence, a redshift measurement of its EM counterpart (either a transient event or a host galaxy) can provide an independent measurement of the Hubble constant [189], and a large spectroscopic catalog of gravitational wave EM counterparts may yield independent H_0 measurements with a precision of few percent [190]. In addition to the direct observation of gravitational wave EM counterparts, cross-correlation of gravitational wave events with spectroscopic galaxy catalogs may also yield improved joint constraints on H_0 [191, 192].

Similarly, the distance to FRBs may also be determined by their dispersion measure [193]. However, this method presents degeneracies with the baryon distribution in the FRB sightline, which in turn allows FRBs to constrain the baryon content of the Universe [194, 195]. Regardless of these degeneracies, measurements of H_0 using FRBs and spectroscopic redshifts of their host galaxies are possible [196, 197]. Therefore, MUST will undoubtedly help with these measurements of H_0 by providing unprecedentedly large spectroscopic redshift catalogs of potential gravitational wave and FRB hosts.

4 Target Selection

We must pay special attention to selecting targets from imaging surveys to achieve the scientific goals outlined in the previous section. There are two main requirements for cosmological target selection: 1) there should be easily identifiable spectral features, such as strong emission lines, absorption features, or continuum breaks, to enable redshift determination with a minimal exposure time; 2) the target density must be optimized to balance the cosmic variance and shot noise to maximize the precision of cosmological measurements. This section explores target selection criteria suitable for MUST and addresses these concerns.

4.1 Challenges of Target Selection for Stage-V Spectroscopic Surveys

Unlike spectroscopic surveys using a prism (e.g., PRIMUS, [198, 199]), grism (e.g., 3D-HST, [200]; Euclid [18]), or IFS (e.g., HETDEX [201]), modern surveys using multi-slit instruments or robotic fiber positioners require careful and sophisticated target selection based on multi-band imaging data. Starting from the Main Galaxy Sample (MGS) in SDSS, primarily a flux-limited sample, the following surveys have gradually increased the number of different samples. As a Stage-IV survey, the main survey of DESI has already included low-redshift bright galaxies (BGS, [202]), luminous red galaxies (LRG, [203]), emission-line galaxies (ELG, [204]), and QSOs ([205]). Selecting these samples now involves more complex selection criteria, including multiple color cuts, cross-matching with multi-wavelength datasets, and the application of machine learning-based methods (e.g., [206, 207]).

These changes reflect the increasingly demanding scientific and operational requirements of modern surveys. A survey must design flexible programs for bright & dark nights and different observing conditions while maximizing the fiber efficiency and the scientific output of the project. More importantly, for LSS redshift surveys, target selection design needs to ensure the volume densities, redshift distributions, and average halo biases of different LSS tracers meet the requirements for constraining the cosmological model. At the same time, the target selection should intentionally reduce the systematics inherited from the imaging surveys, such as the target density fluctuations induced by the variation of imaging depth, observing conditions, Galactic extinction, and data reduction issues. As the number of redshifts rapidly increases, the Stage-IV spectroscopic surveys officially entered the low shot-noise regime, where systematic issues from target selection are becoming critical for the cosmological potential of the survey. Looking forward to the Stage-V era for

Project	Survey Name	Survey Area (deg ²)	Imaging Depth (AB Mag)									Reference
			NUV	<i>u</i>	<i>g</i>	<i>r</i>	<i>i</i>	<i>z</i>	Y	J	H	
CSST	Optical Survey Wide	~ 17,500	25.40	25.40	26.30	26.00	25.90	25.20	24.40			Zhan et al. 2010; Cao et al. 2018; Zhan et al. 2021
	Optical Survey Deep	~ 400	26.70	26.70	27.50	27.20	27.00	26.50	25.70			
Euclid	Wide Survey	~ 14,500				$I_E = 26.20$			24.50	24.50	24.50	Scarmamella et al. 2022
LSST	Wide Fast Deep (WFD)	~ 14,500		25.30	26.84	27.04	26.35	25.22	24.47			DESC et al. 2018 Assuming 1/3 visits of WFD
	North Ecliptic Spur (NES)	~ 4,160			25.64	25.84	25.15	24.02				
UNIONS	UNIONS/CFIS	~ 4,861		24.30	25.20	24.90	24.30	24.10				Ibata et al. 2017
	Extended UNIONS <i>u</i> -band	~ 8,988		24.30								
Legacy Survey	DECaLS	~ 9,000			24.65	23.61	22.84					Dey et al. 2019
	BASS + MzLS	~ 5,000			24.30	23.70	23.04					
Mozi	Wide Field Survey	~ 8,000		24.82	25.85	25.36	24.83	23.90				Wang et al. 2023
HSC SSP	SSP Wide	~ 1,400			26.50	26.50	26.20	25.20	24.40			Aihara et al. 2022
	SSP Deep+UltraDeep	~ 37			27.40	27.10	26.90	26.30	25.30			

Table 2 Summary of available, ongoing, and planned imaging surveys that overlap with the potential footprint of MUST and can contribute to the target selection for LSS tracers of MUST. Please see the reference for details. The imaging depths represent the $5\text{-}\sigma$ point source detection limits. However, we ignore the minor differences in aperture choices and filter differences between surveys. Please see Figure 2 to visualize their footprints.

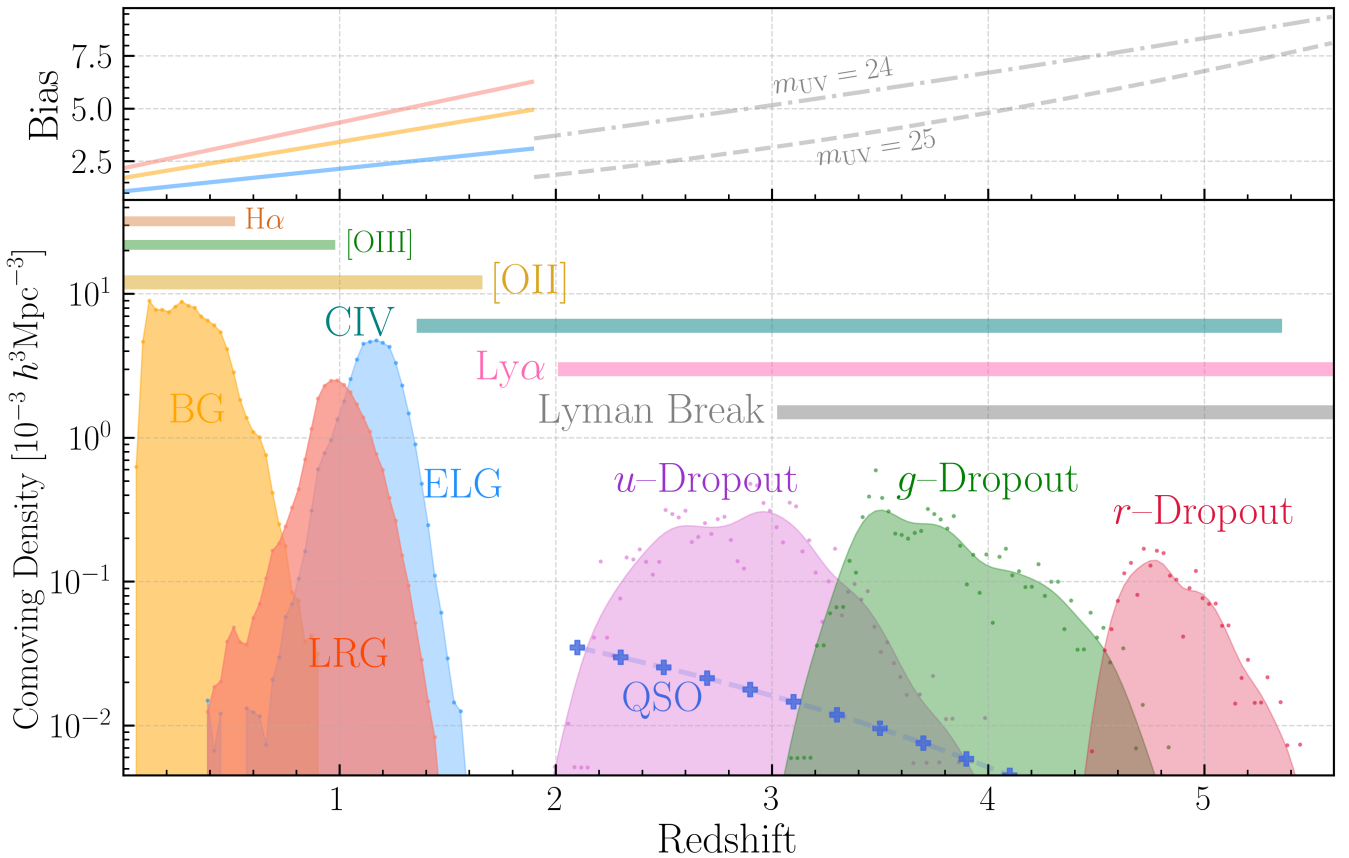


Figure 4 Here, we show the preliminary target selection strategy for the LSS spectroscopic surveys of MUST. The bottom panel shows the redshift distributions and comoving densities of the primary LSS tracers of MUST for low-intermediate redshift ($z < 1.5$) and high-redshift universe. At $z < 1.5$, MUST will densely sample the LSS with the help of low-redshift bright galaxies (BG), luminous red galaxies (LRG), and emission line galaxies (ELG) using their [O II] doublets along with other optical emission lines ([O III], H_β , H_α , etc.) and significant absorption features. Using horizontal bars with distinct colors, we highlight the spectrograph wavelength coverage of different emission lines across the redshift space for MUST. At $z > 2$, MUST plans to utilize the dropout technique to select Lyman Break Galaxies (LBG) in a large comoving volume to map the high- z LSS with unprecedented details. Based on the potential imaging data, we demonstrate the initial target selection results for *u*-, *g*-, and *r*-dropout galaxy selections. The spectrograph of MUST can measure the redshifts of these galaxies using their Lyman break feature, the Lyman- α emission lines, and other strong interstellar absorption lines such as the [C IV] feature. MUST will also observe a large sample of $z > 2$ QSOs as a complementary LSS tracer. The top panel shows the redshift evolution models for the BG, LRG, and ELG at $z < 2$ and a bias model for LBG with different UV magnitude limits. The cosmological forecast presented here is based on these models.

MUST, we will not only anticipate the continued development of these trends but also face new challenges.

In particular, the LSS survey of MUST faces two outstanding challenges. First, the high-redshift ($2 < z < 5$) surveys of Stage-V ask for new LSS tracers that differ from those adopted by the Stage-III and Stage-IV projects, such as the ELG and LRG. The best candidates are Lyman Break Galaxies (LBG) selected using the Lyman-break “dropout” technique and the Lyman- α Emitters (LAEs) traditionally identified in narrow-band imaging surveys. These types of high- z populations, representing galaxies with a wide range of stellar mass, star-formation rate, and halo properties (e.g., halo bias), should be able to continuously cover the redshift range observable by the spectrograph of MUST ($2 < z < 5$) with sufficient tracer densities (e.g., [208]). However, while the high- z galaxy community has been studying these populations extensively for two decades now (e.g., Hu & McMahon 1996 [209]; Cowie & Hu 1998 [210]), we still have not acquired the demanding broad- and narrow-band imaging capabilities to select them for a Stage-V survey and also have not fully understood their cosmological potential as existing deep field studies are still limited by cosmic variance among other systematics. As the LSS survey community has started to pay attention and organize pilot programs (e.g., [21, 211]), we expect to better understand these new LSS tracers before the first light of MUST. The proposed DESI-II project is exciting as it could start the first LSS survey using LBG and LAEs in ~ 2029 , gaining valuable insights before the operation of MUST.

Secondly, given the site selection of MUST in the northern hemisphere, we do not enjoy the deep & uniform multi-band imaging coverage of the Legacy Survey of Space and Time (LSST) of the Vera C. Rubin Observatory in the south. Based on the landscape of imaging surveys in the north, no similar survey will be available before the 2030s. The panel (a) of Figure 2 visualizes the footprints of major imaging surveys that overlap with the potential footprint of MUST and can contribute to the target selection of MUST. We also summarize their survey areas and imaging depths in Table 2. Assuming MUST will observe targets with airmass better than 1.5, at the Lenghu site, MUST can cover the $\delta \geq 10^\circ$ footprint. Within this area, no imaging survey can cover the high Galactic latitude region suitable for an LSS survey. In the ideal scenario, the Chinese Space Station Telescope’s optical survey (CSST-OS) will provide the best multi-band support from the NUV to the Y -band. The NUV and u -band observations are particularly important for selecting $z > 2$ LBG. Meanwhile, the *Euclid* mission will provide valuable near-infrared (NIR) coverage and deep observations in the broad

I_E optical band. While the exact strategy is yet to be investigated, the synergy between optical and NIR images from space should provide unique advantages and new angles for target selection. However, based on the current survey plan, both CSST and *Euclid* will avoid the region near the Ecliptic plane. For this region, the LSST survey should provide partial coverage, but most of it was covered by the Northern Ecliptic Spur (NES) mini-survey⁹⁾ of ([212]), which will only observe in g , r , i , & z -filters with $\sim 1/3$ of the visits of the main Wide-Fast-Deep (WFD) survey. While the coadding depth is still competitive, the lack of u -band is unfortunate for the LBG selection. The ongoing Ultraviolet Near Infrared Optical Northern Survey (UNIONS) campaign using the 3.6 m CFHT, 2×1.8 m Pan-STARRS, and 8.2 m Subaru telescopes is another major candidate for multi-band target selection. In an ideal situation, the southern extension of UNIONS in the u -band to the northern limit ($\delta = +12^\circ$) of the main survey of LSST will be especially valuable.

In addition to these ongoing or planned imaging surveys, we expect the available multi-band data from the Legacy Survey (in g , r , and z -bands; [213]) and the Hyper Suprime-Cam Subaru Strategic Program (HSC-SSP; [153]) will be essential for the development of target selection strategy for MUST: Legacy Survey satisfies the survey footprint requirements for a northern Stage-V project, while HSC-SSP, along with the UNIONS u -band data should meet or surpass the imaging depth requirements for MUST. Also, the 2.5 m Mozi wide-field survey telescope at Peak C of the Lenghu site has started its operation. As a dedicated time-domain survey telescope that will continue its operation into the 2030s, its accumulated imaging depths will also be helpful to MUST. Moreover, the potential of imaging the northern sky using customized narrow- or medium-band filters to facilitate the selection of LAEs is an intriguing opportunity to be explored. We should also mention that CFHT, Subaru, and the 4.0 m Blanco telescope still have wide-field imaging capability that could support imaging campaigns to provide targeting selection support for any Stage-V spectroscopic surveys. In particular, the narrow- and medium-band surveys using the Dark Energy Camera (DECam; [214]), such as the One-hundred-deg² DECam Imaging in Narrowbands (ODIN; [215]), the Merian survey (e.g., [216]), and J-PAS (e.g., [156]) could demonstrate an interesting new approach for target selection for Stage-V survey.

Put all together, we can see that MUST is facing the highly challenging task of developing a consistent target selection strategy that meets the strict requirements for a Stage-V survey. As this work focuses on the theoretical prediction of the potential of LSS cosmology, we will not dive deep into

9) <https://survey-strategy.lsst.io/baseline/minis.html>

the details of target selection as many of the imaging datasets mentioned above have yet to be available. Instead, in the following subsections, we will briefly introduce the concepts and assumptions of target selection for the LSS survey of MUST.

For the cosmological prediction, we will assume two scenarios for the survey footprints: the ideal scenario for the grey (dark) time survey will have a $13,000 \text{ deg}^2$ ($11,000 \text{ deg}^2$) footprint and a more conservative $11,000 \text{ deg}^2$ ($8,000 \text{ deg}^2$) footprint.

4.2 Low-Redshift Tracers

Similar to the ongoing DESI survey, MUST can measure the redshift of $z < 1.57$ galaxies using the [O II] doublet emission lines at 3727 \AA & 3729 \AA , along with the other significant emission and absorption features in galaxies' spectra. While this "low-redshift" component is not the most critical one for the cosmological goals of MUST, it will be a valuable dataset that enables many other complementary cosmological probes, such as the multi-tracer clustering to explore the non-linear regime (e.g., [217, 218]), the cross-correlations with weak lensing surveys like CSST & *Euclid* and other multi-wavelength datasets (e.g., [9, 219, 220]), and the spectroscopic survey of galaxy clusters (e.g., [221, 222]).

For now, we assume that MUST will follow the recipes of DESI to select BGS [202], LRG [203], and ELG [204] samples as $z < 1.6$ LSS tracers. Conceptually, we plan to observe BGS and LRG samples as the bright night targets while observing ELG during the grey and dark nights.

By 2030, DESI and its extension should have finished collecting for more than 40 million redshifts in this range. Therefore, we will only focus on targets fainter than those of DESI. Although the methods are similar, the BGS, LRG, and ELG samples for MUST were selected using photometric data from Legacy Survey DR10.1 instead of DR9. As Legacy Survey DR11 is scheduled to be released in 2025, it would be interesting to check if the samples can be improved with this new release.

4.2.1 Bright Galaxy Sample (BGS)

For the high-density BGS sample, as DESI will have already observed BGS to $r < 20.175 \text{ mag}$ (including the FAINT sub-sample), MUST will observe fainter samples. Assuming that MUST can assign 2,000 fibers per deg^2 to observe BGS during a bright night, based on the target selection results of DESI, MUST will focus on the magnitude range of $20.175 < r < 21 \text{ mag}$ in the Legacy Survey data after making similar quality cleaning cuts in [202]. Firstly, we exclude

stellar objects following [202] using the *Gaia* catalog to perform an additional magnitude cut:

$$G_{\text{Gaia}} - r_{\text{raw}} > 0.6. \quad (4)$$

Then, we use the spatial mask bits provided by Legacy Survey to avoid targets polluted by bright stars in the vicinity. Those are defined as BITMASK 1, 12 and 13. Finally, to clean the sample from spurious objects and to ensure that the selection is based on high-quality observations, we perform the following final cut:

$$\begin{aligned} -1 < (g - r) < 4 \\ -1 < (r - z) < 4, \end{aligned} \quad (5)$$

and we impose that the object has been observed at least once in the g, r and z bands. We have not made any cuts based on fiber magnitude as MUST will adopt a larger fiber size than DESI (1.3 v.s. 1.5 arcsec). We only require the target density and redshift distribution estimate for the cosmological forecast. For BGS, the detailed fiber magnitude or color cut should make little difference at this stage. We will apply them later for more accurate specifications.

In Figure 4, we show that the redshift distribution of the BGS sample ranges between $0.1 < z < 0.8$ with a broad peak between $z = 0.2$ to 0.4 . For the halo bias assumption for the BGS, as this work intends to compare with the forecast of DESI, we adopt the same bias evolution model used in the scientific requirement document of DESI [223]:

$$b(z) = 1.34/D(z) \quad (6)$$

where $D(z)$ is the growth factor that depends on the adopted cosmology [224].

In addition, by reaching $r < 21.5 \text{ mag}$, MUST can increase the target density for BGS by $\sim 2,500 \text{ deg}^{-2}$. Even considering the fiber assignment efficiency and the redshift success rate, which should be higher than 95% given the fiducial exposure time, MUST can easily provide a dense sample of low- z galaxies for various cosmological probes.

4.2.2 Luminous Red Galaxies (LRG)

As their name suggests, LRG represents the massive & (mostly) quiescent galaxies at low-redshift ($z < 0.8$). LRG typically lives in relatively massive dark matter halos with high LSS bias, making them a great candidate to trace the matter distribution and provide high-quality BAO measurement (e.g., [12, 225]). As done for the BGS sample, we follow the LRG target selection recipe of DESI but avoid observing the same targets as the latter by reaching a fainter magnitude limit. DESI adopted the z -band fiber magnitude

$z_{\text{fiber}} < 21.6$ cut as the primary flux-limit cut for LRG. Although MUST will use fiber with a different core size, we use the same Legacy Survey z -band fiber magnitude definition to estimate the sample density and compare it with DESI.

Similar to the BGS, we assume a 2,000 per deg^2 fiber density for LRG as a bright or grey night target. After applying additional quality cleaning cuts as in DESI, we can reach the desired target density using a $21.6 < z_{\text{fiber}} < 22.8$ sample. Firstly, we exclude stars on the $(r - z)$ vs $(z - W1)$ plane:

$$(z - W1) > 0.8 \times (r - z) - 0.6. \quad (7)$$

Then, to obtain targets at $z > 0.4$, we apply a $(g - r)$ vs $(r - W1)$ color cut:

$$(g - W1) > 2.97 \text{ OR } (r - W1) > 1.8. \quad (8)$$

Lastly, we make a color cut on the $(r - W1)$ vs $(W1)$ plane to isolate the most luminous galaxies (in $W1$ band) while keeping the same redshift distribution:

$$\begin{aligned} (r - W1) &> 1.83 \times (W1 - 17.13) \\ (r - W1) &> W1 - 16.31 \text{ OR } (r - W1) > 3.4. \end{aligned} \quad (9)$$

In all the above cuts, $W1$ is the $3.4 \mu\text{m}$ infrared band from the NEOWISE (e.g., [226]) data. Additional cuts to fine-tune the star-galaxy separation are performed by removing non-null proper motion or parallax having a signal-to-noise (SNR) ratio higher than 3 in the *Gaia* EDR3 catalogs. Most *Gaia* detected objects have a magnitude higher than 18 magnitude, making them irrelevant to the LRG selection of MUST. Finally, as for the BGS, we applied the spatial masking BITMASK 1, 12, and 13 and require the object to have a minimum of one valid observation in g , r , z , and $W1$ band.

Figure 4 visualizes the target density and redshift distribution of our LRG selection, which ranges between $0.4 < z < 1.4$ and peaks at $z \sim 1.0$. For the bias evolution model of the LRG, we adopt the DESI one: $b(z) = 1.7/D(z)$.

For LRG, our current z -band fiber magnitude limit approaches the detection limits of Legacy Survey. But, at $z_{\text{fiber}} < 23.0$, MUST can already select a few hundred more LRG per deg^2 to compensate the fiber assignment and redshift measurement to loss to ensure the delivery of a 2,000 deg^{-2} density LRG sample for cosmology. As we reach to fainter magnitude limit, the redshift distribution of the LRG sample for MUST shifts significantly toward a higher average redshift than DESI. As the current selection is still using the LegacySurvey data, it is not clear whether this would be the best option for MUST, which should enjoy deeper imaging data from CSST, LSST, and Euclid. We will explore new approaches to select LRG using imaging data that are better suited to MUST in the upcoming work.

4.2.3 Emission Line Galaxies (ELG)

Emission-line galaxies represent the abundant, active star-forming galaxies at the peak of the cosmic star formation history ($1 < z < 2$). Their high 3-D density and the relative ease to redshift confirmation via the doublet signature of the [O II] emission lines at rest-frame 3727,3729 Å make them appealing $z > 1$ LSS tracers in the Stage-III and IV surveys (e.g., [204,227]). Within the same redshift range, ELG represents the galaxy population that is less massive than the LRG. Therefore, the average halo mass and bias of ELG are systematically lower than LRG. There are also questions about their galaxy-halo connection model (e.g., [228,229]), which could become a systematic for LSS analysis.

Stage-V surveys like MUST can reach a significantly fainter magnitude limit to observe an even larger population of ELG and explore their cosmological potential. Similar to the BGS and LRG samples, we will again follow the ELG selection of DESI in [204] for our forecast. We assume that ELG are grey-time targets with an optimistic 3,600 per deg^2 target density and a conservative 2,500 deg^{-2} density. Compared to the ELG_LOP sample of DESI with a $\sim 1,940 \text{ deg}^{-2}$ density at g -band fiber magnitude brighter than 24.1 mag, we can achieve the desired target density by selecting ELG within the $24.1 < g_{\text{fiber}} < 24.6$ mag range and applying the same color and quality cuts used in DESI. Again, we ignore the difference in fiber core size between MUST and DESI here.

Firstly, DESI designed two $(g - r)$ v.s. $(r - z)$ color cuts to select ELG within the $0.6 < z < 1.6$ redshift range. These cuts also ensure the exclusion of stars while favoring the selection of strong [O II] emitters:

$$\begin{aligned} (g - r) &< 0.5 \times (r - z) + 0.1 \\ (g - r) &< -1.2 \times (r - z) + 1.3, \end{aligned} \quad (10)$$

At the same time, a $(r - z) > 0.15$ color cut is used to exclude $z > 1.6$ galaxies when their [O II] lines redshift out of the wavelength coverage of the spectrograph of DESI, which is very similar to that of MUST.

Similarly, we require the targets to have clean photometry in g , r , and z bands and are not close to a bright star or galaxy using the spatial masking BITMASK 1, 12, and 13.

We show the redshift distribution of ELG and volume density in Figure 4. Since we copied the ELG selection recipe of DESI, it is unsurprising that this sample occupies the identical $0.6 < z < 1.6$ redshift range and peaks at $z \sim 1.2$. We adopt the $b(z) = 0.84/D(z)$ halo bias model for the ELG sample. It is worth noting that while the density of ELG is significantly higher than that of DESI, our current target selection is still based on the relatively shallow LegacySurveys data designed for Stage-IV surveys. Such selection is not optimized

to isolate the targets at higher redshift, which should be the main focus of MUST. Deeper imaging data will improve that. Also, given the anticipated decrease of spectrograph throughput at $\lambda < 9000 \text{ \AA}$, the redshift success rate for faint ELG at the higher end of their redshift distribution strongly depends on the EW of the [O II] emission lines. We will search for improved color selections to isolate the strong-[O II] emitters at $z > 1$.

4.3 High-Redshift Tracers

Starting from $z = 2.1$, the Lyman- α emission line at rest-frame 1216 \AA redshifts into the wavelength coverage at $\sim 370 \text{ nm}$ for the spectrograph of MUST and enables our high-redshift target selection for the Stage-V cosmological survey. Along with the Lyman break feature at rest-frame 912 \AA and a series of interstellar absorption lines, such as C II 1335 \AA , CIV 1548 \AA , O I 1302 \AA + Si II 1304 \AA , and more (e.g., [21, 230]), support the redshift measurements at $2.1 < z < 5.0$ of MUST. High- z LSS tracers are the bread and butter of a Stage-V cosmological survey like MUST. Until the Stage-IV surveys such as DESI, high- z QSOs are the primary LSS tracers at $z > 2$ (e.g., [231-234]). While these accreting supermassive black holes (SMBHs) present us the unique opportunity to explore the inter-galactic medium (IGM) to constrain the nature of dark matter (e.g., [147, 235, 236]), their volume density is typically too low to become the principal LSS tracer in the Stage-V era.

Right now, the most promising candidates of $z > 2$ LSS tracers are the LBG and LAEs (e.g., [21, 208, 211, 237]). Compared to LAEs, selecting LBG based on the broad-band color criteria makes it easier to populate the $2 < z < 5$ redshift space continuously with sufficient density. Given the available data and previous works, we focus on the LBG populations as the primary LSS tracers for our cosmological forecast in this work. While not included in the Fisher forecast, we briefly discuss the potential for LAEs and QSOs.

We should note that LBG and LAEs are defined photometrically, not physically, with overlaps between these two populations. In fact, the success rate of redshift measurement for LBG strongly depends on the presence of a prominent Lyman- α emission line that often makes them LAEs.

4.3.1 Lyman-Break Galaxies (LBG)

LBG are galaxies with significant flux decrement, or a “break”, at the rest-frame wavelength shorter than the Lyman limit (911.3 \AA) due to strong internal absorption by neutral Hydrogen. They represent the “normal”, young, star-forming high redshift galaxies (e.g., [238-241]) with a large enough density to support LSS surveys. In observation, this break

often translates into the non-detection in filters bluer than the observed frame of the Lyman limit (or a “dropout”) or a high color value using filters that put the break between them. Starting from [238], this method and its further development have helped select millions of LBG as candidates of high- z galaxies in $2 < z < 7$ (e.g., ~ 4.1 million from the Great Optically Luminous Dropout Research Using Subaru HSC, or GOLDRUSH project [242]). This mature approach is the foundation of high- z LSS tracer selection using deep broad-band imaging surveys for Stage-IV and Stage-V surveys.

Motivated by the target selection for the proposed DESI-II, [21] validated the LBG selections based on a series of dropout criteria from the HSC SSP and the CLAUDS data using dedicated DESI campaigns and confirmed a $\sim 620 \text{ deg}^{-2}$ $r < 24.2 \text{ mag}$ LBG density at $2.3 < z < 3.5$ or a $\sim 470 \text{ deg}^{-2}$ $r < 24.5 \text{ mag}$ LBG density at $2.8 < z < 3.5$. Also aimed at the fixed $1,100 \text{ deg}^{-2}$ target density for DESI-II, [22] applies a Random Forest selection to the HSC+CLAUDS data and spectroscopically confirmed a 493 deg^{-2} $z > 2.5$ under the imaging depth afforded by a UNIONS-like survey.

In [237], the authors considered the BX color selection in [243] centered at $z \sim 2.20$, the u -dropout selection based on the CFHTLS-Archive-Research-Survey (CARS; [244, 245]) centered at $z \sim 2.96$, and the g - & r -dropout selection based on GOLDRUSH centered at $z \sim 3.8$ & 4.9 . Based on LSST-Y10’s imaging depths, the authors concluded that it is practical to spectroscopically confirm $2,000 R < 24.0 \text{ mag}$ BX galaxies, $500 i < 24.0 \text{ mag}$ u -dropouts, $330 i < 25.5 \text{ mag}$ g -dropouts, and $100 z < 25.5 \text{ mag}$ r -dropouts per square degree. Altogether, this supports a $\sim 3,000 \text{ deg}^{-2}$ confirmed high- z tracers that match the multiplex capability of MUST nicely. Interestingly, the authors point out that the u -band imaging depth limits the photometric selection of u -dropout. This assumes that one needs an actual detection in the u -band (or the band on the bluer side of the observed frame Lyman limit) to estimate the $u - g$ color to identify the break reliably, which is different from the dropout selections used to study the LBG populations (e.g., their luminosity function). It is worth investigating whether this is required to select LSS tracers with straightforward systematics. This is particularly important for MUST as heterogeneous imaging datasets will contribute to our target selection. In this work, we still assume that detection is optional in the band X to select the X -dropout populations.

In the WST Science White Paper [42], the authors estimated the relations between the surface densities of u -, g -, and r -dropouts down to different magnitude limits (see Figure 65): at $r_{\text{lim}} < 24.5 \text{ mag}$, the available photometric density of u -dropout should be within $1,500$ to $2,000 \text{ deg}^{-2}$ for MUST. And, at $i_{\text{lim}} < 24.6$, there are $\sim 1,000 \text{ deg}^{-2}$ g -dropout for MUST to target. For r -dropout, the expected candidate den-

sity is ~ 300 (600) deg^{-2} for a $z_{\text{lim}} < 24.5$ (25.0) mag sample. These values represent the most optimistic estimations for MUST. In reality, the photometric selection will include contamination from galaxies outside of the desired redshift range. MUST will not be able to measure the redshifts of all candidates as the success rate should strongly depend on the presence and the strength of the Ly α emission line.

For the cosmological forecast here, we will not go into the details of the target selection as we do not yet have the multi-band images and spectroscopic validation data required for a definitive Stage-V selection strategy. Instead, based on the previous work, we provide optimistic and conservative number density estimates for each population. For u -dropout in $2.1 < z < 3.5$, we assume that a $r < 24.5$ selection could result in a $1,200 \text{ deg}^{-2}$ sample in an optimistic and a 600 deg^{-2} sample in a conservative situation. For g -dropout in $3.3 < z < 4.5$, we expect a 800 deg^{-2} and 300 deg^{-2} sample for the optimistic and conservative scenarios. As for the r -dropout in $4.5 < z < 5.5$, we assume the optimistic sample has a 200 deg^{-2} density, while the conservative sample halves this value. We summarize these assumptions in Table 2. We do not include the BX selection sample in our forecast as it was defined using a different series of broad-band filters than the Sloan $ugriz$ ones [246]. Hence, the BX criteria require filter conversions to work on the imaging data for MUST or need to be updated. Moreover, the BX-selected sample often centers at $z \sim 2$, leading to a significant fraction out of the redshift range covered by MUST. Still, the current estimation suggests that the potential LSS tracer density at $z < 2.5$ can be much higher when better selection criteria are designed.

To provide the initial estimates of the redshift distributions for each population, we adopt a simple method based on the COSMOS2020¹⁰ photometric and photo- z catalog [247]. Following the previous dropout-selection recipes, we designed the color cuts for the magnitude-limited samples for MUST to roughly reach the desired target density while ensuring their photometric redshift distribution is consistent with the design. We apply the bright object masks from the COSMOS field of the HSC-SSP Ultra-Deep survey. It results in a 1.5 deg^2 effective footprint to estimate the target density. We confirm that the choice of photometric measurements and the photo- z estimations do not affect the derived redshift distribution.

For the u -dropouts, we recover a $\sim 1,500 \text{ deg}^{-2}$ sample within $22.4 < r < 24.5$ mag using the following criteria:

$$\begin{aligned} (u - g) &> 0.95 \\ -0.5 &< (g - r) < 1.1 \\ (u - g) &> 1.17 \times (g - r) + 0.71. \end{aligned} \quad (11)$$

About 88% of the target has photo- z within $2.2 < z < 3.5$ and shows a clear peak at $z = 3$. We confirm that, while using different choices of ugr or ugi color cuts can change the target density from ~ 800 to $>2,000 \text{ deg}^{-2}$, the redshift distribution does not vary significantly.

For the g -dropouts, we design the following grz color cuts to select a $\sim 870 \text{ deg}^{-2}$ sample peaked at $z \sim 3.4$. $\sim 84\%$ of the sample falls into $3.2 < z < 4.5$ based on photo- z , resulting in a $\sim 760 \text{ deg}^{-2}$ sample within $23.0 < i < 24.6$ mag:

$$\begin{aligned} (g - r) &> 1.0 \\ (g - r) &> 1.2 \times (r - z) + 0.65, \end{aligned} \quad (12)$$

As for the r -dropouts, we can define a $23.0 < z < 25.0$ mag sample within $4.0 < z < 5.5$, centered at $z \sim 4.5$ using these riz color cuts:

$$\begin{aligned} (r - i) &> 0.65 \\ -0.5 &< (i - z) < 0.9 \\ (r - i) &> 1.5 \times (i - z) + 0.65, \end{aligned} \quad (13)$$

Using photo- z , this sample has a $\sim 390 \text{ deg}^{-2}$ density within the desired redshift range. Like the u -dropouts, tweaking these preliminary color cuts can significantly change the target density but will not affect the redshift distributions. We want to emphasize that these color cuts are *not* designed for actual target selection, but only to support our *assumptions* for a more optimistic high- z LSS tracer selection in the 2030s.

LBG will be the highest priority target for the dark time program of MUST. However, based on the empirical estimation of the required exposure time (e.g., [42, 237]) for LBG and the results from recent DESI campaigns (e.g., [21, 22]), successfully recover redshifts down to $r \sim 24.5$ mag or deeper is still a challenging task for a 6.5 m telescope. Not only does this challenge demand a careful scientific requirements rundown to guide the design of the scientific instruments, but it also motivates us to investigate an improved selection strategy that focuses on LBG with a clear Ly α emission line. As the throughput of the telescope, fiber, and detector all drop significantly toward the blue end at $\lambda < 4500 \text{ \AA}$, we expect the redshift success rate for u -dropout also reflects this at $z < 2.5$. Given that we have not yet included the BX selection with a high target density, in principle, MUST should be able to guarantee the 3-D tracer density for cosmology at $z < 2.5$. More importantly, despite the uncertainties around the fiber assignment and redshift efficiencies for LBG, the contract between our optimistic and conservative target density estimation should make our cosmological forecast more realistic for MUST.

10) <https://astroweaver.github.io/project/cosmos2020-galaxy-catalog/>

4.3.2 Lyman- α Emitters (LAE)

LAEs are high- z galaxies with strong ($EW \geq 20 \text{ \AA}$) Lyman- α emission lines (e.g., [248]), which are typically young, star-forming galaxies with low stellar and dust mass. As LAEs live in dark matter halos with lower average halo mass than LBG, their potential density should be significant enough to make them competitive high-redshift LSS tracers. In [211], the authors spectroscopically confirm 822 (1,099) $z = 2.40 \pm 0.03$ (3.10 ± 0.03) LAEs in the 8.90 (9.34) deg^2 ODIN fields using the N419 (N501) narrow-band filters down to 25.5 (25.7) $5\text{-}\sigma$ detection limit. These samples correspond to a $\sim 10^{-3} h^{-1} \text{Mpc}^{-3}$ 3D density in two narrow redshift windows, higher than the optimistic prediction of LBG 3D density across the whole redshift range. If such performance can be extrapolated to a broader redshift range, LAEs can become an extremely interesting LSS tracer: not only do they dramatically improve the density of high- z LSS tracers, but their halo bias should also be significantly lower than the dropout-selected LBG (e.g., $b \sim 1.7$ and 2.0 for the two ODIN samples), making multi-tracer probe potentially possible at high- z .

However, due to their faint continuum emission and the limited number of spectral features (often just the Ly α line), the selection of LAEs demands deep narrow-band imaging (e.g., [215]) or IFS (e.g., [249]) observations. Most ongoing LAE surveys either cover much smaller areas than the MUST footprint (e.g., ODIN; [215]) or are not deep enough for MUST (e.g., JPAS; [250, 251]). Furthermore, the bias of LAEs has only been measured on relatively small fields ($\leq 100 \text{deg}^2$, e.g., [211, 252]). We do not include LAEs in our current cosmological forecast for these reasons. At the same time, this implies that the cosmological constraining power of MUST could be further enhanced when a wide & deep LAE sample becomes available in the future. We should note that the DECam on the 4 m Blanco telescope (e.g., [214]) and the HSC on the 8.2 m Subaru (e.g., [153, 154]) can carry out deep narrow- or medium-band surveys in the following years. It is worth noting that DESI has conducted pilot spectroscopic observations of LAEs, demonstrating their promise as LSS tracers of the high-redshift Universe.

4.3.3 Quasi-Stellar Objects (QSO)

Quasi-stellar objects (QSOs) or quasars¹¹⁾ are both direct tracers of the dark matter field and sources for Lyman- α forest detections. The transition in their usage – from tracers to sources – is typically set around $z \sim 2$, depending on their comoving densities. QSOs have been an essential in-

redient of major spectroscopic surveys as the primary targets for probing the $z \gtrsim 2$ Universe. The Stage-III and IV spectroscopic surveys, such as BOSS [253], eBOSS [254], and DESI [205, 255], define the modern standard of QSO target selection using multi-band deep imaging data and broadband color cuts to isolate quasar candidates from stars and other galaxies (e.g., [256-264]). At the same time, these surveys have explored QSO selection based on their flux variability (e.g., [265]) and using machine learning algorithms (e.g., [205, 266, 267]).

While QSOs will certainly enable a wide range of interesting scientific topics in the age of Stage-V surveys, their low 3D density and color degeneracy with abundant Milky Way stars at $z > 2$ (e.g., see Figure 4) make them a less appealing LSS tracers. Therefore, we do not include QSO in the Fisher forecast to constrain cosmological parameters. In Figure 4, we adopt the pure luminosity function evolution model in [265] to estimate the 3D density of QSOs at $r < 23.5$. Assuming 80% of the QSOs will be observed, MUST will reach a QSO density of ~ 310 per deg^{-2} with $\sim 90 \text{deg}^{-2}$ at $z > 2.1$, including the QSOs already observed by BOSS/eBOSS and DESI ($\sim 60 \text{deg}^{-2}$ at $z > 2.1$).

It is worth noting that, while not being the most promising high- z LSS tracers, at $z > 2.1$, QSOs provide the vital capability for studying the IGM using the Ly α forest, which contains intriguing cosmological potential such as constraining the nature of dark matter. We will forecast the potential of Ly α -QSO and provide a more thorough discussion in the following work of this series.

4.4 Summary of the Targets Selection

In Table 3, we summarize the preliminary target selection discussed above and provide an initial estimate of the survey cost measured using the total fiber-hour. All but the QSO samples are considered in the cosmological forecast.

The effective collecting area of MUST will be $\sim 3.2\times$ than the one for DESI¹²⁾. Considering the additional throughput loss caused by the secondary mirror, WFC, fiber route, and spectrograph, we assume that for the same target, MUST can reach the same S/N $2.5\times$ faster than DESI. This ignores the difference caused by seeing (Lenghu site is likely to have better median seeing than Kitt Peak) and fiber core diameter (1.5 arcsec for DESI v.s. 1.3 arcsec for MUST). For the same target type, MUST will observe fainter targets than DESI. We assume the exposure time will increase $10^{2\delta m/2.5}$ times for the fainter sample, where δm is the magnitude difference. We assume DESI can achieve the designed redshift success rate

11) We use the term QSO and quasar interchangeably in this work.

12) We assume the primary mirror of DESI is 3.8 m in diameter with a 1.8 m central obscuration. For MUST, we assume the central obscuration has a 2.5 m central obscuration

Sample Name	Magnitude Limit (AB mag)	Redshift Distribution	Angular Density (deg ⁻²)	Number of Redshift Bins	3D Density (10 ⁻³ h ³ Mpc ⁻³)	Bias Value	Survey Area (deg ²)	T _{Exp} (Hour)	Total Number of Redshift (10 ⁶)	Total Fiber Hours (10 ⁶)
BGS	20.18 < r < 21.0	0.1 < z < 0.7	2,000	2	5.7	1.6	~13,000	0.12	26.0	3.12
LRG	21.6 < z _{fib} < 22.8	0.8 < z < 1.3	2,000	2	1.0	2.8	~13,000	1.00	26.0	26.0
ELG	24.1 < g _{fib} < 24.6	0.8 < z < 1.4	Opt:3,600	2	1.49	1.5	~13,000	0.30	46.8	14.0
			Con:2,500	2	1.03	1.5	~11,000	0.30	27.5	8.25
u-Dropout	22.4 < r < 24.5	2.2 < z < 3.5	Opt:1,200	3	0.21	4.5	~11,000	2.50	15.6	39.0
			Con:600	3	0.11		~8,000	2.50	6.0	15.0
g-Dropout	23.0 < i < 24.6	3.2 < z < 4.5	Opt:800	2	0.16	5.3	~11,000	6.00	10.4	62.4
			Con:300	2	0.06		~8,000	6.00	3.0	18.0
r-Dropout	23.0 < z < 25.0	4.0 < z < 5.5	Opt:200	1	0.06	6.4	~11,000	8.00	2.6	20.8
			Con:100	1	0.03		~8,000	8.00	1.0	8.0
QSO	r < 23.5	z > 2.1	90				~13,000	0.12	1.2	0.14

Table 3 Summary of the low- and high-redshift samples selected in this work. All but the QSO samples are considered in the cosmological forecast. For the ELG, *u*-, *g*-, and *r*-dropout galaxies, we estimate an optimistic (“Opt”) and conservative (“Con”) surface density to design the survey.

using 200 seconds of exposure time for BGS and 1,000 seconds of exposure time for LRG, ELG, and QSO. Hence, we estimate that MUST can achieve the same 95% to 99% redshift success rate using 440, 3600, 729, and 440 seconds of exposure time for BGS, LRG, ELG, and QSO.

Estimating the exposure time for the LBG is more difficult. Based on the recent LBG observation campaign by DESI [21], for a $r < 24.2$ mag *u*-dropout sample, DESI can already achieve a ~ 70 redshift efficiency in 2.5-hour of exposure time. However, the efficiency seems to plateau after 2.5-hour hours as a 5-hour exposure still cannot improve it to $> 80\%$. It is worth noting that there is certainly room to improve the LBG redshift estimation soon with the arrival of better spectral models or templates. So, for the *u*-dropout sample, we apply the simple empirical scaling relation and assume that MUST can achieve the same success rate for our $r < 24.5$ mag sample with a 2.5-hour exposure. For the *g*- and *r*-dropouts, it is less straightforward to estimate the required exposure time as there is no statistically meaningful DESI sample to compare with. In [237], the authors estimated an 80-minute exposure would be enough for a $z = 24$ mag galaxy using a 6.5 m telescope. Scaling this up to a $z < 24.50$ mag sample would require a 3.4-hour exposure time.

4.5 Conceptual Survey Design

This section briefly describes the conceptual survey designs for the bright-grey and dark-time programs of MUST based on the previous description of the telescope & instrument design and the target selection under several oversimplified assumptions. In the upcoming work of this series, we will present a more proper survey design backed by detailed instrument specifications, an exposure time calculator (ETC) for MUST, and an improved target selection strategy.

4.5.1 Dark Time Survey

We assume that the CSST photometry will support the selection of dark-time targets for MUST, which will mainly include the LBG at $2.2 < z < 5.0$. The right panel of Figure 5 shows a preliminary observing pattern. Each single pointing represents the 5 deg² effective FoV of MUST. Given the latitude of the Lenghu site, MUST can not observe the whole footprint for CSST. Assuming a maximum of 1.5 airmass ($\sim 40^\circ$ above the horizon) for observation, we cut the footprint at Dec $> -10^\circ$. Observing 11 000 deg² or 2600-pointing observations (with a minimal overlap for a continuous coverage) and with an average of 2.5 hours exposure per target, this represents a total of 650 effective nights of dark time with an average 10/nights. Assuming a 70% clear night fraction and 35% of Dark Time during the year and accounting for 80% survey efficiency, this translates into a 7.5-year observing program. Altogether, a total of about 30 million redshift measurements should be obtained during this dark-time survey, assuming an overall 70% redshift measurement efficiency.

4.5.2 Grey Time Survey

As the grey time program will primarily focus on BGS, LRG, and ELG, we use the Legacy Survey footprint to simulate the pointings needed for MUST as shown in the left panel of Fig.5. With the limitation in declination, MUST can observe a total of $\sim 13\,000$ deg² of the Legacy Survey footprint, corresponding to ~ 3100 contiguous MUST pointings.

With an average of 1.0 hours exposure per target with a target density of ~ 2 times the fiber density for MUST ($\sim 4,000$ deg⁻²; this could include 2,000 deg⁻² BGS, 2,000 deg⁻² LRG, 3,600 deg⁻² ELG, and 400 deg⁻² of other targets), such survey represents a total of 620 effective nights of grey time with 10 hours per night. Assuming 40% of Grey Time during the year, accounting for 80% survey efficiency, and a 70%

clear night fraction, this translates into a 6.0-year observing program. Altogether, the grey-time program of MUST can accumulate ~ 88 million redshift measurements during this time, assuming an overall 85% redshift measurement efficiency. Among these grey-time targets, the exposure time required for LRG (~ 1 hour for a $z_{\text{fiber}} = 22.8$ mag target) is significantly longer than the others. With a careful survey strategy, the average exposure time per grey-time target could be shortened to speed up the current program, leaving space for further increase of the grey-time target density. For example, within the current detection limits of the LegacySurveys, we could select BGS down to $r < 21.5$ mag with a $\sim 4,000$ deg^{-2} density, LRG down to $z_{\text{fiber}} = 23.0$ mag with a $\sim 3,000$ deg^{-2} density. Combining them with the current ELG sample will result in a target density $\sim 2.7\times$ the fiber density. Assuming a 1.0 hour *average* exposure time, this project will take ~ 8.3 -year of grey-time to finish with a ~ 114 million redshifts at $z < 1.6$ with an 80% average redshift efficiency. Safely assuming a fraction of these grey-time targets can be observed during bright time, it is possible to finish this along with the 7.5-year dark-time survey.

Given the required length of the dark-time program, an extension of the grey-night program down to a fainter magnitude limit could reach a target density of 3 times the fiber density of MUST. Assuming a 75% overall redshift success rate, MUST can obtain a total of ~ 93 million redshifts during a 7.0-year grey-time survey.

Putting the grey & dark programs together, MUST has the capability of collecting ~ 120 million redshifts at $0.1 < z < 5.0$ before 2040.

5 Cosmological Forecasts

To quantitatively evaluate the scientific potential of MUST in addressing the fundamental cosmological questions outlined in Section 3, we perform forecasts for the statistical errors associated with several key science cases based on the expected target densities and biases detailed in Section 4. To highlight potential improvements offered by MUST, we compare our forecasts with those for DESI, the current state-of-the-art Stage-IV survey, using the target specifications given by [223]. In particular, we focus on DESI galaxy samples, including BGSs, LRG, and ELG. Furthermore, to comprehensively assess the scientific potential of next-generation cosmological data, we include external priors from CMB surveys, including Planck [268] and the Simons Observatory (SO; [45]), following the strategy detailed in [16].

5.1 Methodology

The Fisher forecast method is widely used to estimate the statistical uncertainty of cosmological parameters inferred from the observed power spectrum. This method is based on the Cramér-Rao inequality [269, 270], which establishes that no unbiased estimator can achieve a covariance matrix smaller than the inverse of the Fisher information matrix \mathbf{F} . It follows that the standard deviation of the i -th measured parameter θ_i is bounded from below by $\sigma(\theta_i) \geq \sqrt{(F^{-1})_{ii}}$. Following the formulation in [271], the Fisher information matrix for a redshift survey can be approximated as

$$F_{ij} \sim \frac{\partial \mathbf{P}^T}{\partial \theta_i} \mathbf{C}^{-1} \frac{\partial \mathbf{P}}{\partial \theta_j}, \quad (14)$$

where \mathbf{P} is the data vector with $P_i = P(k_i, \mu_i)$ representing the power spectrum of the i -th bin in \mathbf{k} -space, and \mathbf{C} is the associated covariance matrix of the power spectrum. With the usual assumption that the overdensity field is approximately a Gaussian random field, the covariance matrix \mathbf{C} is given by

$$C_{ij} \sim \delta_{ij} \frac{2P_i^2}{V_i V_{\text{eff}}}, \quad (15)$$

where V_i is the volume of the i -th bin in \mathbf{k} -space, and V_{eff} is the effective survey volume.

Throughout this work, we perform Fisher forecasts using the tracer power spectrum $P(\mathbf{k})$, with

$$k_{\text{max}} = 0.4 h \text{ Mpc}^{-1}, \quad (16)$$

which can be computed using either full-shape models or a template-based manner. However, we use Bayesian inference to estimate error for forecasts related to dark matter constraints. For the full-shape model, we make use of the forecast tool FishLSS¹³, which is described in detail in [16]. FishLSS computes the nonlinear tracer power spectrum using Lagrangian perturbation theory with a linear tracer bias model, further refined by fitting a single-parameter counterterm to the HaloFit prescription. Shot noise and the finger-of-god effect are incorporated based on the density of the tracers. The template-based approach is only used for the $f\sigma_8$ forecasts (Section 5.3). In this approach, we adopt a code¹⁴ developed in a recent forecast for redshift surveys [272], which refers to the RSD template developed by [273].

The number densities and biases of different tracers used for our forecasts are detailed in Table 3. We perform two sets of forecasts – optimistic and conservative – based on the different estimations of available imaging data to ensure a comprehensive evaluation of the scientific potential of MUST.

13) <https://github.com/NoahSailer/FishLSS>

14) https://github.com/wdoumerg/Forecast_highz_spectroscopic_survey

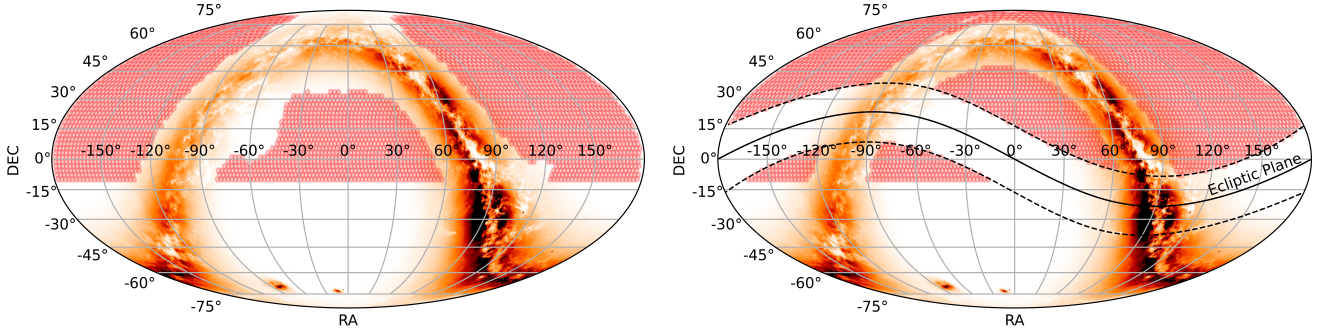


Figure 5 Example of an observation sequence. Each red circle represents the footprint of MUST (5 deg²). **Left:** grey time based on the DECaLS footprint modified by a cut on declination (Dec > -10°). **Right:** dark time based on the CSST footprint. We get a total of 3100 and 2600 pointings reaching ~13 000 and 11 000 deg², respectively. On both maps, the stellar density of the Milky Way is represented using a white-red color map, and the Ecliptic plane region is highlighted in black on the right panel.

5.2 Dark Energy

As a critical driver of cosmic expansion history, dark energy – particularly its dynamic behavior – can be unveiled by geometrical measurements, with BAO as the standard ruler (see Section 3.1). The BAO scale corresponds to the sound horizon at the drag epoch, r_d , and is linked to the angular separation $\Delta\theta$ and redshift separation Δz of tracer pairs that exhibit excess correlation in the transverse and line-of-sight directions, respectively:

$$r_d = (1+z)D_A(z)\Delta\theta = \Delta\theta \int_0^z \frac{cdz'}{H(z')}, \quad (17)$$

$$r_d \approx \frac{c\Delta z}{H(z)}, \quad (18)$$

where $D_A(z)$ denotes the angular diameter distance and $H(z)$ is the Hubble parameter. Thus, the BAO feature permits measurements of the combinations $D_A(z)/r_d$ and $H(z)r_d$ as functions of redshift.

Figure 6 shows the errors on α_\perp and α_\parallel from different spectroscopic surveys, which can be interpreted as deviations in $D_A(z)/r_d$ and $H(z)r_d$ measurements from the expected values in the fiducial cosmology. The top panels show Fisher forecast results for MUST tracers across different redshifts, where the upper and lower boundaries of the shaded regions correspond to results based on the conservative and optimistic target density estimations, respectively. The error bars in the bottom panels are all evaluated in the optimistic scenario, with the red lines representing predictions of the best-fit flat- w_0w_a CDM model based on the combination of DESI Y1, CMB, and DES Y5 data [73], illustrating how distance measurements can differentiate between dark energy models.

The precision in distance measurements of MUST is generally at the percent level with the assumption of a fiducial Λ CDM cosmology, demonstrating strong potential for constraining the equation of state. In the local Universe ($z < 0.7$), MUST provides constraints comparable to existing surveys

due to the limitation of cosmic variance. In the intermediate redshift range, the ELG samples of MUST are expected to yield significantly tighter constraints. Furthermore, MUST offers access to LBGs at unprecedentedly high redshift $z \gtrsim 2$, although constraints are limited in this regime due to the low dark energy density. However, by combining tracers among all redshift, MUST is anticipated to achieve a much tighter constraint on the model of dark energy.

5.3 Structure Growth & Gravity

The distinction between GR and alternative gravity models can be inferred through measurements of structure growth derived from the anisotropic galaxy clustering, often parameterized by $f\sigma_8$ (see Section 3.2). Figure 7 shows Fisher forecasts for the statistical errors of $f\sigma_8$ with MUST tracers, based on RSD measurements with template power spectra, compared with constraints from some existing surveys. Overall, MUST is expected to achieve more than a 4-fold improvement in precision at $z < 1.6$, thanks to its high galaxy number density. Furthermore, MUST LBG will enable measurements of $f\sigma_8$ in the high-redshift Universe ($z > 2$) that is largely unexplored before.

As shown in the bottom panel, in the optimistic case, MUST will be able to constrain structure formation with 2%-level precision across all redshift bins up to $z \sim 5$, with the only exception of ~4% for BGS at $z < 0.4$, possibly due to unavoidable cosmic variance given the limited volume. The conservative estimation mainly affects the constraints of high- z LBGs, resulting in a ~3–4% precision. In any case, the unprecedented precision of structure growth measurements enables a significant potential for testing gravity theories with MUST data. Assuming a fiducial GR- Λ CDM framework, several gravity theories currently consistent with the state-of-the-art spectroscopic data – with their best-fitting parameters – could potentially be ruled out by MUST. For instance, with

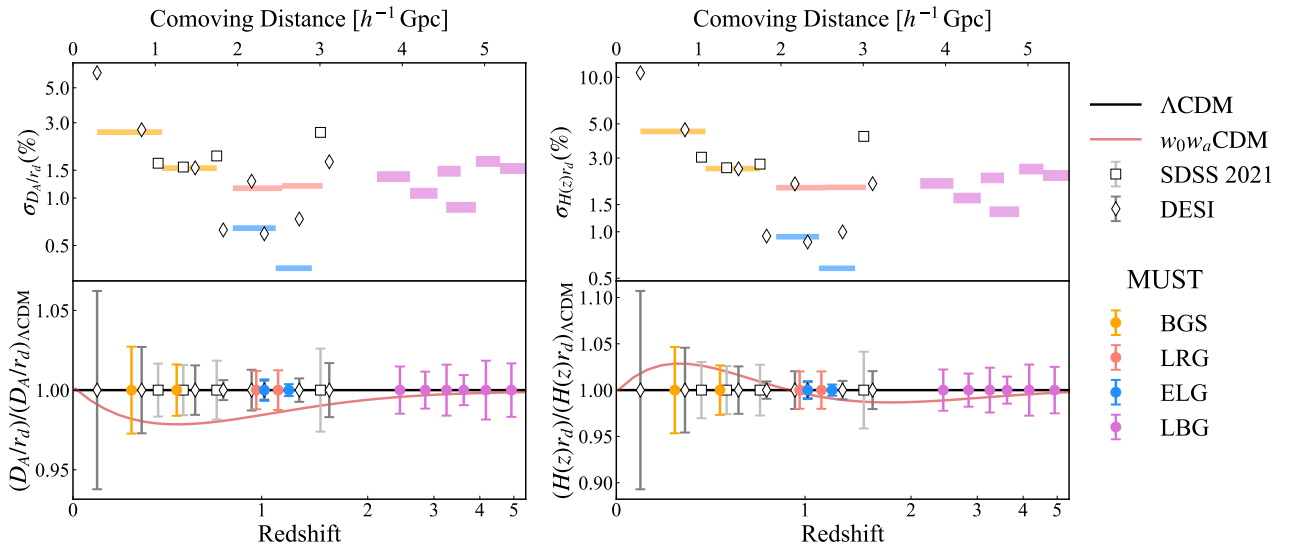


Figure 6 Top panels: errors on $D_A(z)r_d$ (left) and $H(z)r_d$ (right) from SDSS measurements [10] and our forecasts for DESI and MUST galaxies. The lower and upper limits of the shaded regions show the estimation with optimistic and conservative MUST observational conditions, respectively. Bottom panels: the same errors are centred on the flat- Λ CDM cosmology, in comparison with deviations from Λ CDM for the best-fit flat- w_0w_a CDM model suggested by the DESI Y1 data [73].

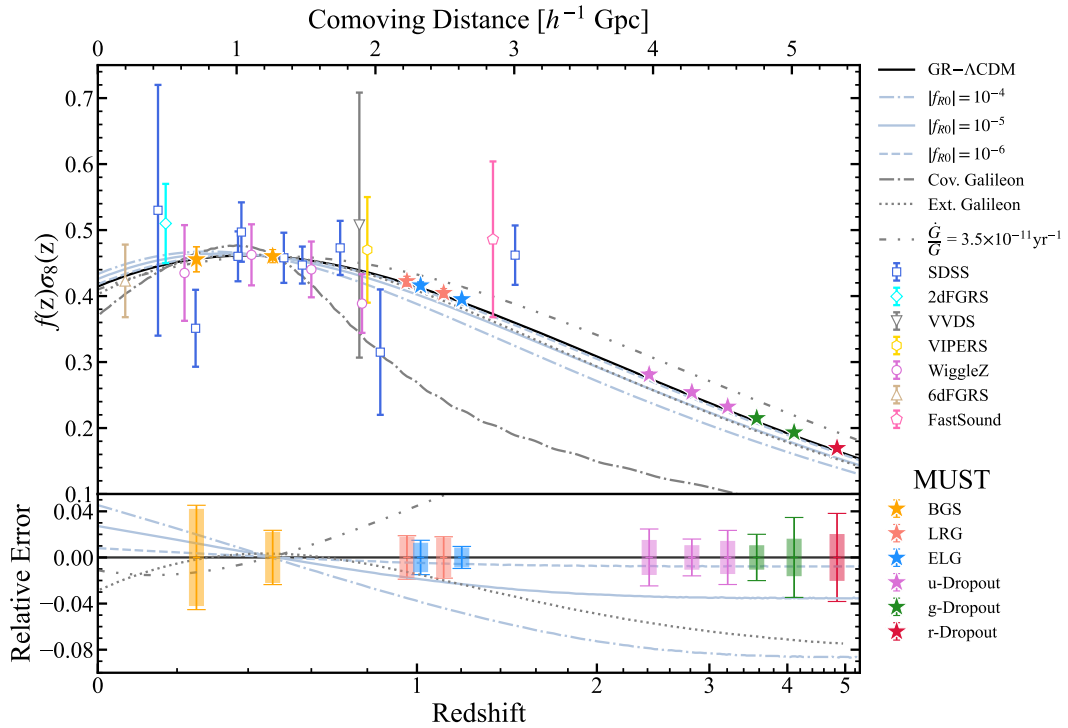


Figure 7 Top panel: Fisher forecast for $f\sigma_8$ measurements of MUST at different redshifts. Bottom panel: Relative error of MUST measurements and the deviation of different gravity models to the fiducial GR- Λ CDM model. The shaded regions represent the optimistic scenario, while the lines indicate the more conservative forecast. Results from existing surveys are shown with open symbols on the top panel: SDSS [10, 274, 275], 2dFGRS [276], VVDS [277], VIPERS [278], WiggleZ [279], 6dFGRS [280], FastSound [281]. In both panels, MUST targets are indicated by filled stars color-coded based on the galaxy sample. The black solid line denotes the GR- Λ CDM model. In contrast, other lines represent several alternative gravity theories: the covariant Galileon gravity [282], the extended Galileon gravity [283], the varying gravitational constant model with $|\dot{G}/G| = 3.5 \times 10^{-11} \text{yr}^{-1}$ [284], and the $f(R)$ model [285] with $|f_{R0}| = 10^{-4}$, 10^{-5} , and 10^{-6} .

notable contributions of constraints at $z > 2$, MUST is expected to probe $|f_{R0}|$ of $f(R)$ gravity down to the 10^{-6} level.

5.4 Primordial Non-Gaussianity

The presence of PNG incorporates a form of dependence on the initial potential field, ϕ , into the galaxy bias model [286]. At first order, this dependence adds a so-called "scale-dependent bias" term to the galaxy power spectrum

$$P_{\text{gg}}(k, z) = \left(b_1 + f_{\text{NL}}^{\text{local}} b_\phi \frac{3H_0^2 \Omega_m}{2k^2 T(k) D_{\text{md}}(z)} \right)^2 P_{\text{mm}}(k, z) + P_{\text{shot}}(z), \quad (19)$$

where $b_1(z)$ denotes the linear galaxy bias, $b_\phi(z)$ represents the galaxy bias on ϕ , $T(k)$ is the transfer function and $D_{\text{md}}(z)$ is the linear growth factor normalized to $1/(1+z)$ at the matter-dominated epoch. $T(k)$ is normalized to 1 on large scales, where the PNG signal is the most prominent, so the "scale-dependent" effect typically follows a k^{-2} behavior. In our current forecasts, we focus exclusively on the local-shape configuration and apply a commonly used universality relation, $b_\phi = 2\delta_c(b_1 - 1)$, where δ_c is the critical density in the spherical collapse model. Recent studies, however, suggest that this relation may vary depending on the specific galaxy sample [287, 288], and we leave further investigations to future works.

Our forecast results are presented in Fig. 8. For comparison, we perform similar forecasts for DESI and show the existing constraints from BOSS and Planck. Notably, an independent constraint from MUST is expected to limit $f_{\text{NL}}^{\text{local}}$ to a precision of $\sigma(f_{\text{NL}}^{\text{local}})$ ranging from 1.83 to 2.08, providing a five-fold improvement over DESI and outperforming the state-of-the-art CMB constraint of $\sigma(f_{\text{NL}}^{\text{local}}) = 5.1$ from Planck [97]. Moreover, the combined constraints from MUST and CMB will tighten the limit to $1.48 < \sigma(f_{\text{NL}}^{\text{local}}) < 1.68$. Additional methodologies not included in this forecast, such as the multi-tracer approach [289] and bispectrum [290], are anticipated to further enhance MUST's capability to $\sigma(f_{\text{NL}}^{\text{local}}) < 1.0$, which is crucial from a theoretical perspective, as a non-detection at this level would rule out many models involving the curvaton mechanism [95, 291].

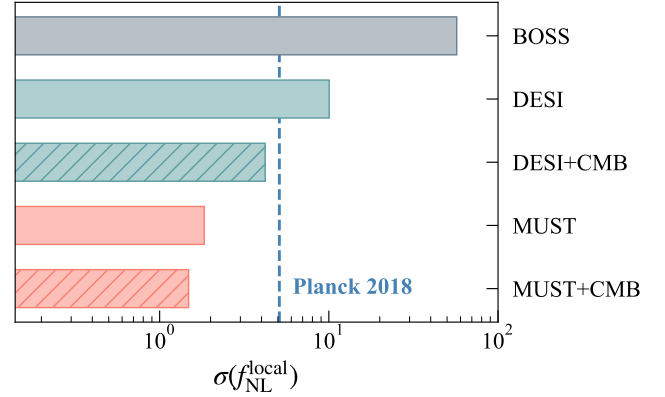


Figure 8 The $1\text{-}\sigma$ constraints on $f_{\text{NL}}^{\text{local}}$ from LSS surveys include BOSS (gray, see Table B1 in [292]) and our forecasts for DESI (green) and MUST (red, dark and light for the optimistic and conservative estimations respectively). The state-of-the-art constraint from Planck is shown as the blue dashed line for comparison. The slashed bars indicate the constraints combining the constraints from Planck [268] low- ℓ and Simons Observatory (SO; [45]) high- ℓ measurements.

5.5 Neutrinos

The impacts of neutrinos on the expansion history of the Universe and the structure formation process permit constraints on the total neutrino mass M_ν through galaxy clustering measurements (see Section 3.4). As a Stage-V spectroscopic survey with high tracer number density and extensive survey volume, MUST is expected to place stringent constraints on neutrino mass and potentially distinguish between the normal and inverted mass hierarchies when combined with CMB measurements.

We present a Fisher forecast for the error on M_ν derived from joint constraints of MUST and CMB measurements, assuming a fiducial value of $M_\nu = 0.06$ eV within the Λ CDM framework, as shown in Figure 9. Under the assumption of a normal mass hierarchy, where neutrinos consist of a single massive eigenstate and two massless states, the statistical error, ranging from 0.31 eV in the optimistic estimation and 0.40 eV in the conservative case, is expected to enable the detection of a nonzero neutrino mass with $> 1.5\sigma$ CL, which significantly enhances the best constraint from Planck with $\sigma(M_\nu) = 0.11$ eV. The inverted mass hierarchy can also be tested with a significance of $> 1.0\sigma$.

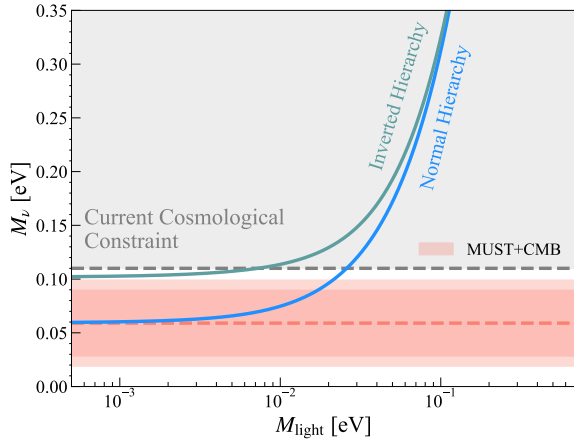


Figure 9 Fisher forecast for the total neutrino mass M_ν based on the galaxy power spectrum with $k_{\max} = 0.4 h \text{ Mpc}^{-1}$. Solid lines represent the variation of M_ν , with the mass of the lightest neutrino species in both mass hierarchies: inverted hierarchy (green) and normal hierarchy (blue). The red dashed line indicates the fiducial cosmology with $M_\nu = 0.06 \text{ eV}$, while the dark (light) red-shaded region represents the optimistic (conservative) 1σ uncertainty. The gray dashed line marks the upper limit of M_ν by combining the CMB and BAO data from Planck [293].

5.6 Warm Dark Matter

The Ly α forest is a powerful tool for probing small-scale structures and constraining dark matter models with small-scale cutoffs. When accounting for the repercussions of inhomogeneous H I reionization [149], the Ly α forest power spectrum can differentiate between various dark matter models even on large scales ($k \lesssim 0.6 h \text{ Mpc}^{-1}$) (Zhang et al. in prep.). Here, we focus on warm dark matter models whose characteristic suppression of small-scale structure mirrors that of other dark matter models with similar small-scale cutoffs. We forecast the ability of MUST to place competitive constraints on warm dark matter particle mass by leveraging the reionization imprints in the Ly α forest power spectrum. Following [149], the flux power spectrum is given by

$$P_F^{3D}(\mathbf{k}, z, m_X) = b_F^2(1 + \beta_F \mu^2)^2 P_m + 2b_F b_\Gamma(1 + \beta_F \mu^2) P_{m,\psi}, \quad (20)$$

where b_F and β_F are the bias coefficient and redshift-space distortion parameters, respectively. b_Γ is the radiation bias [294], $\mu \equiv k_{\parallel}/k$, and $P_{m,\psi}$ is the cross-power spectrum of matter and transparency of the IGM, which correspond to the response of the IGM to reionization.

The second term in Eq. (20) enables us to relate the small-scale suppression caused by warm dark matter models during reionization to a distinct large-scale signature, i.e., the impact of inhomogeneous reionization on the Ly α . These reionization relics are coupled to the scale of the ionized bubbles, spanning a few Mpc to tens of Mpc. On such large

scales, the dependence of the bias coefficients and the need for non-linear modeling concerning m_X can be reasonably disregarded.

We use Monte Carlo Markov Chain (MCMC) implemented with EMCEE [295] to forecast the constraints on warm dark matter mass m_X by MUST. In addition to m_X , we include σ_8 as a free parameter to account for potential degeneracies. We consider 12 redshift bins from 2.0 to 3.8 and 45 k -bins spanning 0.09 to $0.67 h \text{ Mpc}^{-1}$. We use an estimated quasar luminosity function for MUST with $r < 23.5$ and consider different survey areas. We follow [296, 297] to compute the corresponding covariance, which includes an aliasing term that accounts for the sparse sampling of quasars. Figure 10 showcases the constraining power of MUST across three survey areas ($5,000$, $10,000$, and $14,000 \text{ deg}^2$). An optimistic survey area of $14,000 \text{ deg}^2$ would yield the most stringent constraint on warm dark matter mass to date: $m_X > 10.5 \text{ keV}$ (at 95% confidence level). Even a conservative $10,000 \text{ deg}^2$ survey would yield $m_X > 7.6 \text{ keV}$, exceeding the current strongest constraint from the Ly α forest alone, $m_X > 5.7 \text{ keV}$ [146].

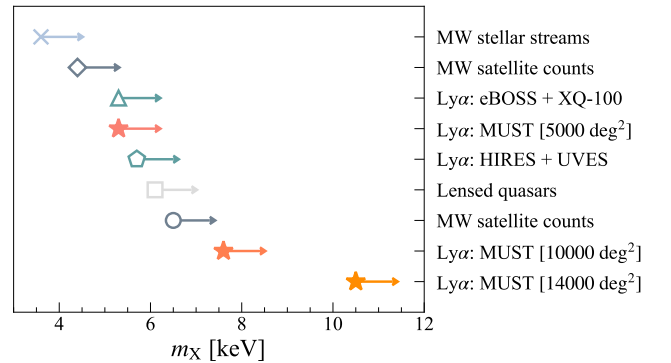


Figure 10 Warm dark matter constraints. Arrows indicate the allowed parameter space (not the associated error), which extends towards infinity, representing CDM. Forecasted MUST constraints using the Ly α forest for the warm dark matter mass are highlighted by stars for different survey areas. For context, we include representative constraints from MW stellar streams [298], MW satellite counts [299, 300], Lyman- α forest measured by eBOSS + XQ-100 [145] and by HIRES + UVES [146], as well as strongly lensed quasars from JWST [301].

6 Conclusions

The MULTIplexed Survey Telescope (MUST) is a 6.5-meter telescope dedicated to multi-object spectroscopic observations. It features a modularized focal plane with 336 triangular modules that accommodate over 20,000 fibers at the Cassegrain focus. The spectrographs are designed with three channels to cover a wavelength range of ~ 3700 – 9600 \AA at a resolution of $R \sim 2000$ – 4000 . Initial monitoring of observ-

ing conditions indicates that the MUST candidate site, Peak A of the Saishiteng Mountain near Lenghu Town, could provide over 2,400 observing hours annually, making MUST at least 10 times more efficient than currently operating spectroscopic surveys. As a result, MUST is expected to collect over 100 million spectra in the 2030s.

While designed as a flexible spectroscopic platform, the primary mission of MUST is to conduct the first Stage-V galaxy spectroscopic survey¹⁵⁾ to address fundamental questions in cosmology and physics. With its unprecedented photon collecting capability as a spectroscopic telescope, MUST will produce the first 3D map of galaxies spanning from the nearby Universe out to $z \sim 5.5$, which corresponds to ~ 1 billion years after the Big Bang. This large survey volume enables in-depth studies of the dynamic evolution of the dark Universe and signals of fundamental physics in the primordial Universe. Thus, the primary scientific objectives of MUST include investigating the nature and evolution of dark energy, testing gravity theories, probing inflation physics through primordial non-Gaussianity, exploring properties of neutrinos and dark matter, etc.

Different types of targets are required to cover the extensive redshift range with sufficient density to achieve these ambitious scientific goals. For the low-redshift Universe ($z \lesssim 1.6$), MUST will use the same galaxy targets and similar selection criteria as DESI but will focus on fainter samplers to avoid redundant observations. Beyond $z \sim 2$, MUST will mainly rely on LBG and LAEs to map large-scale structures. Although the actual target selection and redshift measurement efficiencies are not yet fully verified, current multi-band imaging and spectroscopic validation data in limited areas suggest that these tracers will be abundant enough for precise cosmological inferences. Meanwhile, QSOs will play a vital complementary role in probing the IGM, which is crucial for studying specific physical effects, such as the mass of dark matter particles.

We have performed forecasts for some key scientific motivations of MUST. At low redshifts ($z \lesssim 1.6$), the increased galaxy density provides stringent constraints on geometric measurements with percent-level precision for nearly all tracers, demonstrating the potential to distinguish between dark energy models. Meanwhile, the $z \gtrsim 2$ galaxies significantly enhance the constraining power of structure growth measurements, reaching 2 %-level precision at most redshifts, thus enabling robust tests of gravity models. With the MUST data, we foresee that constraints on the primordial non-Gaussianity parameterized by $f_{\text{NL}}^{\text{local}}$ from LSS data will surpass the precision of Planck measurements for the first time. Combined with CMB data from Planck and Simons Observatory, MUST

could achieve $f_{\text{NL}}^{\text{local}}$ measurements with precision on the order of unity, highlighting its potential in probing primordial physics. The combination of MUST and CMB data further gives a statistical error on the total neutrino mass of ~ 0.03 eV, enabling evidence of non-zero neutrino mass confirmation. Additionally, with the Lyman- α forest data, MUST will be able to set a lower limit of warm dark matter mass of ~ 10.5 keV when assuming 14,000 deg² survey area, exceeding current best constraints. These forecasts demonstrate that, once completed, the MUST spectroscopic survey will contribute substantially to addressing fundamental cosmological and physical questions.

The MUST project is supported by the Ministry of Science and Technology, China (Grant No. 2023YFA1605600) and the Ministry of Education, China.

We want to express our sincere gratitude to Mr. Tian-Pei Chen for his generous donation and unwavering trust, which has significantly supported the MUST project. We also thank Mr. Dong-Hua Dong for his donation.

The authors thanks Noah Sailer, Anand Raichoor, Ji Yao for useful discussions.

Song Huang acknowledges the support from the National Natural Science Foundation of China (NSFC) Grant No. 12273015 & No. 12433003 and the China Crewed Space Program through its Space Application System.

JPK, AR, DF, JY, AV, RG, and SH acknowledge the support from the SNF 200020.175751 and 200020.207379 "Cosmology with 3D Maps of the Universe" research grant.

Si-Wei Zou acknowledges the support from the National Science Foundation of China (No. 12303011).

Yu Liu acknowledges the support from the National Science Foundation of China (No. 12303005) and the Shuimu Tsinghua Scholar Program (No. 2022SM173).

Pablo Renard acknowledges the support by the Tsinghua Shui Mu Scholarship, funding of the National Key R&D Program of China (grant no. 2023YFA1605600), the science research grants from the China Manned Space Project with No. CMS-CSST2021-A05, the Tsinghua University Initiative Scientific Research Program (No. 20223080023), and the National Science Foundation of China (grant no. 12350410365).

Conflict of interest The authors declare that they have no conflict of interest.

- 1 J. Huchra, M. Davis, D. Latham, and J. Tonry, *ApJS***52**, 89 (1983).
- 2 V. de Lapparent, M. J. Geller, and J. P. Huchra, *ApJ***302**, L1 (1986).
- 3 C. L. Bennett, D. Larson, J. L. Weiland et al., *ApJS***208**, 20 (2013), arXiv: [1212.5225](https://arxiv.org/abs/1212.5225).
- 4 Planck Collaboration, N. Aghanim, Y. Akrami et al., *A&A***641**, A6 (2020), arXiv: [1807.06209](https://arxiv.org/abs/1807.06209).
- 5 D. Scolnic, D. Brout, A. Carr et al., *ApJ***938**, 113 (2022), arXiv: [2112.03863](https://arxiv.org/abs/2112.03863).
- 6 M. Betoule, R. Kessler, J. Guy et al., *A&A***568**, A22 (2014), arXiv: [1401.4064](https://arxiv.org/abs/1401.4064).
- 7 DES Collaboration, T. M. C. Abbott, M. Acevedo et al., arXiv e-prints **973**, arXiv:2401.02929 (2024), arXiv: [2401.02929](https://arxiv.org/abs/2401.02929).

¹⁵⁾ proposed by the Snowmass Cosmic Frontier report [75] as a continuation of the stages defined by the Dark Energy Task Force [15]

- 8 T. M. C. Abbott, M. Aguena, A. Alarcon et al., *Phys. Rev. D* **105**, 023520 (2022), arXiv: [2105.13549](#).
- 9 C. Heymans, T. Tröster, M. Asgari et al., *A&A* **646**, A140 (2021), arXiv: [2007.15632](#).
- 10 S. Alam, M. Aubert, S. Avila et al., *Phys. Rev. D* **103**, 083533 (2021), arXiv: [2007.08991](#).
- 11 DESI Collaboration, B. Abareshi, J. Aguilar et al., *AJ* **164**, 207 (2022), arXiv: [2205.10939](#).
- 12 D. J. Eisenstein, I. Zehavi, D. W. Hogg et al., *ApJ* **633**, 560 (2005), arXiv: [astro-ph/0501171](#).
- 13 N. Kaiser, *MNRAS* **227**, 1 (1987).
- 14 DESI Collaboration, A. G. Adame, J. Aguilar et al., arXiv e-prints arXiv:2404.03000 (2024), arXiv: [2404.03000](#).
- 15 A. Albrecht, G. Bernstein, R. Cahn et al., arXiv e-prints astro-ph/0609591 (2006), arXiv: [astro-ph/0609591](#).
- 16 N. Sailer, E. Castorina, S. Ferraro, and M. White, *J. Cosmology Astropart. Phys.* **2021**, 049 (2021), arXiv: [2106.09713](#).
- 17 H. Zhan, *Chinese Sci. Bull.* **66**, 1290 (2021), URL <https://www.sciengine.com/10.1360/TB-2021-0016>.
- 18 Euclid Collaboration, Y. Mellier, Abdurro'uf et al., arXiv e-prints arXiv:2405.13491 (2024), arXiv: [2405.13491](#).
- 19 D. Spergel, N. Gehrels, J. Breckinridge et al., arXiv e-prints arXiv:1305.5422 (2013), arXiv: [1305.5422](#).
- 20 Ž. Ivezić, S. M. Kahn, J. A. Tyson et al., *ApJ* **873**, 111 (2019), arXiv: [0805.2366](#).
- 21 V. Ruhlmann-Kleider, C. Yèche, C. Magneville et al., *J. Cosmology Astropart. Phys.* **2024**, 059 (2024), arXiv: [2404.03569](#).
- 22 C. Payerne, W. d'Assignies Doumerg, C. Yèche et al., arXiv e-prints arXiv:2410.08062 (2024), arXiv: [2410.08062](#).
- 23 J. McCullough, D. Gruen, A. Amon et al., *MNRAS* **531**, 2582 (2024), arXiv: [2309.13109](#).
- 24 S. Samuroff, R. Mandelbaum, J. Blazek et al., *MNRAS* **524**, 2195 (2023), arXiv: [2212.11319](#).
- 25 C. Lamman, D. Eisenstein, J. N. Aguilar et al., *MNRAS* **522**, 117 (2023), arXiv: [2209.03949](#).
- 26 R. C. Wolf, C. B. D'Andrea, R. R. Gupta et al., *ApJ* **821**, 115 (2016), arXiv: [1602.02674](#).
- 27 M. T. Soumagnac, P. Nugent, R. A. Knop et al., arXiv e-prints arXiv:2405.03857 (2024), arXiv: [2405.03857](#).
- 28 J. Koda, C. Blake, T. Davis et al., *MNRAS* **445**, 4267 (2014), arXiv: [1312.1022](#).
- 29 K. Said, C. Howlett, T. Davis et al., arXiv e-prints arXiv:2408.13842 (2024), arXiv: [2408.13842](#).
- 30 E. Kitanidis and M. White, *MNRAS* **501**, 6181 (2021), arXiv: [2010.04698](#).
- 31 J. Myles, A. Alarcon, A. Amon et al., *MNRAS* **505**, 4249 (2021), arXiv: [2012.08566](#), URL <https://dx.doi.org/10.1093/mnras/stab1515>.
- 32 S. Yuan, C. Blake, A. Krolewski et al., *MNRAS* **533**, 589 (2024), arXiv: [2403.00915](#).
- 33 J. U. Lange, C. Blake, C. Saulder et al., *The Open Journal of Astrophysics* **7**, 57 (2024), arXiv: [2404.09397](#).
- 34 S. Chen, J. DeRose, R. Zhou et al., arXiv e-prints arXiv:2407.04795 (2024), arXiv: [2407.04795](#).
- 35 M. Amiri, K. Bandura, T. Chen et al., *ApJ* **947**, 16 (2023), arXiv: [2202.01242](#).
- 36 C. L. Chang, L. Newburgh, D. Shoemaker et al., arXiv e-prints arXiv:2209.08265 (2022), arXiv: [2209.08265](#).
- 37 J. Annis, J. A. Newman, and A. Slosar, arXiv e-prints arXiv:2209.08049 (2022), arXiv: [2209.08049](#).
- 38 D. J. Schlegel, J. A. Kollmeier, G. Aldering et al., arXiv e-prints arXiv:2209.04322 (2022), arXiv: [2209.04322](#).
- 39 G. A. Blanc, J. H. Silber, S. Smee et al., in *Ground-based and Airborne Telescopes IX*, (edited by H. K. Marshall, J. Spyromilio, and T. Usuda), volume 12182 of *Society of Photo-Optical Instrumentation Engineers (SPIE) Conference Series*, 1218230 (2022).
- 40 S. Asai, A. Ballarino, T. Bose et al., arXiv e-prints arXiv:2407.19176 (2024), arXiv: [2407.19176](#).
- 41 A. Sheinis, S. C. Barden, and J. Sobek, *Astronomische Nachrichten* **344**, e20230108 (2023), arXiv: [2307.07667](#).
- 42 V. Mainieri, R. I. Anderson, J. Brinchmann et al., arXiv e-prints arXiv:2403.05398 (2024), arXiv: [2403.05398](#).
- 43 D.-q. Su, H. Bai, X. Yuan, and X. Cui, *Science China Physics, Mechanics, and Astronomy* **67**, 279511 (2024), arXiv: [2310.04697](#).
- 44 Y. Zhang, H. Jiang, S. Shectman et al., *PhotoniX* **4**, 16 (2023).
- 45 N. Galitzki, A. Ali, K. S. Arnold et al., in *Millimeter, Submillimeter, and Far-Infrared Detectors and Instrumentation for Astronomy IX*, (edited by J. Zmuidzinas and J.-R. Gao), volume 10708 of *Society of Photo-Optical Instrumentation Engineers (SPIE) Conference Series*, 1070804 (2018), arXiv: [1808.04493](#).
- 46 K. N. Abazajian, P. Adshead, Z. Ahmed et al., arXiv e-prints arXiv:1610.02743 (2016), arXiv: [1610.02743](#).
- 47 LiteBIRD Collaboration, E. Allys, K. Arnold et al., *Progress of Theoretical and Experimental Physics* **2023**, 042F01 (2023), arXiv: [2202.02773](#).
- 48 Square Kilometre Array Cosmology Science Working Group, D. J. Bacon, R. A. Battye et al., *PASA* **37**, e007 (2020), arXiv: [1811.02743](#).
- 49 J. B. Oke and J. E. Gunn, *ApJ* **266**, 713 (1983).
- 50 D. J. Schlegel, S. Ferraro, G. Aldering et al., arXiv e-prints arXiv:2209.03585 (2022), arXiv: [2209.03585](#).
- 51 G. Marchiori, S. De Lorenzi, L. Ghedin et al., in *Ground-based and Airborne Telescopes X*, (edited by H. K. Marshall, J. Spyromilio, and T. Usuda), volume 13094 of *Society of Photo-Optical Instrumentation Engineers (SPIE) Conference Series*, 1309439 (2024).
- 52 P. Li, Z. Wang, S. Huang et al., *Optics Express* **32**, 20931 (2024).
- 53 X. Xing, C. Zhai, H. Du, W. Li, H. Hu, R. Wang, and D. Shi, in *Advanced Technology Optical/IR Telescopes VI*, (edited by L. M. Stepp), volume 3352 of *Society of Photo-Optical Instrumentation Engineers (SPIE) Conference Series*, 839–849 (1998).
- 54 G. Smith, J. Brzeski, S. Mizziarski, P. R. Gillingham, A. Moore, and A. McGrath, in *Astronomical Structures and Mechanisms Technology*, (edited by J. Antebi and D. Lemke), volume 5495 of *Society of Photo-Optical Instrumentation Engineers (SPIE) Conference Series*, 348–359 (2004).
- 55 M. Akiyama, S. Smedley, P. Gillingham et al., in *Advanced Optical and Mechanical Technologies in Telescopes and Instrumentation*, (edited by E. Atad-Ettdugui and D. Lemke), volume 7018 of *Society of Photo-Optical Instrumentation Engineers (SPIE) Conference Series*, 70182V (2008).
- 56 N. F. Staszak, J. Lawrence, D. M. Brown et al., in *Advances in Optical and Mechanical Technologies for Telescopes and Instrumentation II*, (edited by R. Navarro and J. H. Burge), volume 9912 of *Society of Photo-Optical Instrumentation Engineers (SPIE) Conference Series*, 99121W (2016).
- 57 J. Brzeski, G. Baker, S. Baker et al., in *Ground-based and Airborne Instrumentation for Astronomy VII*, (edited by C. J. Evans, L. Simard, and H. Takami), volume 10702 of *Society of Photo-Optical Instrumentation Engineers (SPIE) Conference Series*, 1070279 (2018).
- 58 M. Schubnell, J. Ameel, R. W. Besuner et al., in *Ground-based and Airborne Instrumentation for Astronomy VI*, (edited by C. J. Evans, L. Simard, and H. Takami), volume 9908 of *Society of Photo-Optical Instrumentation Engineers (SPIE) Conference Series*, 990892 (2016).
- 59 M. Rombach, X. Xu, R. Araujo et al., in *Ground-based and Airborne Instrumentation for Astronomy X*, (edited by J. J. Bryant, K. Motohara, and J. R. D. Vernet), volume 13096 of *Society of Photo-Optical Instrumentation Engineers (SPIE) Conference Series*, 130969V (2024).
- 60 L. Deng, F. Yang, X. Chen et al., *Nature* **596**, 353 (2021).
- 61 JUST Team, C. Liu, Y. Zu et al., *Astronomical Techniques and Instruments* **1**, 16 (2024), arXiv: [2402.14312](#).
- 62 Planck Collaboration, A. Abergel, P. A. R. Ade et al., *A&A* **571**, A11

- (2014), arXiv: [1312.1300](#).
- 63 Planck Collaboration, P. A. R. Ade, N. Aghanim et al., *A&A***594**, A13 (2016), arXiv: [1502.01589](#).
- 64 A. G. Riess, A. V. Filippenko, P. Challis et al., *AJ***116**, 1009 (1998), arXiv: [astro-ph/9805201](#).
- 65 S. Perlmutter, G. Aldering, G. Goldhaber et al., *ApJ***517**, 565 (1999), arXiv: [astro-ph/9812133](#).
- 66 S. M. Carroll, W. H. Press, and E. L. Turner, *ARA&A***30**, 499 (1992).
- 67 L. Perivolaropoulos and F. Skara, *New A Rev.***95**, 101659 (2022), arXiv: [2105.05208](#).
- 68 E. J. Copeland, M. Sami, and S. Tsujikawa, *International Journal of Modern Physics D* **15**, 1753 (2006), arXiv: [hep-th/0603057](#).
- 69 D. J. Eisenstein and W. Hu, *ApJ***496**, 605 (1998), arXiv: [astro-ph/9709112](#).
- 70 O. H. E. Philcox, B. D. Sherwin, G. S. Farren, and E. J. Baxter, *Phys. Rev. D***103**, 023538 (2021), arXiv: [2008.08084](#).
- 71 F. Dong, C. Park, S. E. Hong, J. Kim, H. S. Hwang, H. Park, and S. Appleby, *ApJ***953**, 98 (2023), arXiv: [2305.00206](#).
- 72 S. Cole, W. J. Percival, J. A. Peacock et al., *MNRAS***362**, 505 (2005), arXiv: [astro-ph/0501174](#).
- 73 DESI Collaboration, A. G. Adame, J. Aguilar et al., arXiv e-prints arXiv:2404.03002 (2024), arXiv: [2404.03002](#).
- 74 X. Wang, G. Gu, X. Mu, S. Yuan, and G.-B. Zhao, *Research in Astronomy and Astrophysics* **24**, 065002 (2024), arXiv: [2404.06310](#).
- 75 A. S. Chou, M. Soares-Santos, T. M. P. Tait et al., arXiv e-prints arXiv:2211.09978 (2022), arXiv: [2211.09978](#).
- 76 D. Huterer, *A&A Rev.***31**, 2 (2023), arXiv: [2212.05003](#).
- 77 A. J. S. Hamilton, in *The Evolving Universe*, (edited by D. Hamilton), volume 231 of *Astrophysics and Space Science Library*, 185 (1998), arXiv: [astro-ph/9708102](#).
- 78 Y.-S. Song and W. J. Percival, *J. Cosmology Astropart. Phys.***2009**, 004 (2009), arXiv: [0807.0810](#).
- 79 G.-B. Zhao, T. Giannantonio, L. Pogosian et al., *Phys. Rev. D***81**, 103510 (2010), arXiv: [1003.0001](#).
- 80 T. M. C. Abbott et al. (DES), *Phys. Rev. D* **107**, 083504 (2023), arXiv: [2207.05766](#).
- 81 K. S. Dawson, J.-P. Kneib, W. J. Percival et al., *AJ***151**, 44 (2016), arXiv: [1508.04473](#).
- 82 P. McDonald, *J. Cosmology Astropart. Phys.***2009**, 026 (2009), arXiv: [0907.5220](#).
- 83 A. Achúcarro, M. Biagetti, M. Braglia et al., arXiv e-prints arXiv:2203.08128 (2022), arXiv: [2203.08128](#).
- 84 J. Ellis and D. Wands, arXiv e-prints arXiv:2312.13238 (2023), arXiv: [2312.13238](#).
- 85 Planck Collaboration, Y. Akrami, F. Arroja et al., *A&A***641**, A10 (2020), arXiv: [1807.06211](#).
- 86 R. Flauger, L. McAllister, E. Pajer, A. Westphal, and G. Xu, *J. Cosmology Astropart. Phys.***2010**, 009 (2010), arXiv: [0907.2916](#).
- 87 X. Chen and M. H. Namjoo, *Physics Letters B* **739**, 285 (2014), arXiv: [1404.1536](#).
- 88 X. Chen, *Advances in Astronomy* **2010**, 638979 (2010), arXiv: [1002.1416](#).
- 89 P. D. Meerburg, D. Green, R. Flauger et al., *BAAS***51**, 107 (2019), arXiv: [1903.04409](#).
- 90 D. Karagiannis, T. Shanks, and N. P. Ross, *MNRAS***441**, 486 (2014), arXiv: [1310.6716](#).
- 91 M. S. Cagliari, E. Castorina, M. Bonici, and D. Bianchi, Optimal constraints on Primordial non-Gaussianity with the eBOSS DR16 quasars in Fourier space (2024), arXiv: [2309.15814](#).
- 92 R. Scoccimarro, L. Hui, M. Manera, and K. C. Chan, *Phys. Rev. D***85**, 083002 (2012), arXiv: [1108.5512](#).
- 93 W. R. Coulton, F. Villaescusa-Navarro, D. Jamieson et al., *ApJ***943**, 178 (2023), arXiv: [2206.15450](#).
- 94 J. Maldacena, *Journal of High Energy Physics* **2003**, 013 (2003), arXiv: [astro-ph/0210603](#).
- 95 M. Kawasaki, T. Kobayashi, and F. Takahashi, *Phys. Rev. D***84**, 123506 (2011), arXiv: [1107.6011](#).
- 96 Y.-F. Cai, W. Xue, R. Brandenberger, and X. Zhang, *J. Cosmology Astropart. Phys.***2009**, 011 (2009), arXiv: [0903.0631](#).
- 97 Planck Collaboration, Y. Akrami, F. Arroja et al., *A&A***641**, A9 (2020), arXiv: [1905.05697](#).
- 98 N. Dalal, O. Doré, D. Huterer, and A. Shirokov, *Phys. Rev. D***77**, 123514 (2008), arXiv: [0710.4560](#).
- 99 D. Green, Y. Guo, J. Han, and B. Wallisch, *J. Cosmology Astropart. Phys.***2024**, 090 (2024), arXiv: [2311.04882](#).
- 100 X. Chen and Y. Wang, *Phys. Rev. D***81**, 063511 (2010), arXiv: [0909.0496](#).
- 101 N. Arkani-Hamed and J. Maldacena, arXiv e-prints arXiv:1503.08043 (2015), arXiv: [1503.08043](#).
- 102 P. D. Meerburg, M. Münchmeyer, J. B. Muñoz, and X. Chen, *J. Cosmology Astropart. Phys.***2017**, 050 (2017), arXiv: [1610.06559](#).
- 103 G. Cabass, O. H. E. Philcox, M. M. Ivanov, K. Akitsu, S.-F. Chen, M. Simonović, and M. Zaldarriaga, arXiv e-prints arXiv:2404.01894 (2024), arXiv: [2404.01894](#).
- 104 W. Sohn, D.-G. Wang, J. R. Fergusson, and E. P. S. Shellard, arXiv e-prints arXiv:2404.07203 (2024), arXiv: [2404.07203](#).
- 105 S. Navas, C. Amsler, T. Gutsche et al., *Phys. Rev. D***110**, 030001 (2024).
- 106 M. Aker, D. Batzler, A. Beglarian et al., arXiv e-prints arXiv:2406.13516 (2024), arXiv: [2406.13516](#).
- 107 J. Lesgourgues and S. Pastor, *Phys. Rep.***429**, 307 (2006), arXiv: [astro-ph/0603494](#).
- 108 J. Lesgourgues and S. Pastor, arXiv e-prints arXiv:1212.6154 (2012), arXiv: [1212.6154](#).
- 109 Y. Du and J.-H. Yu, *Journal of High Energy Physics* **2021**, 58 (2021), arXiv: [2101.10475](#).
- 110 P. F. de Salas, S. Gariazzo, P. Martínez-Miravé, S. Pastor, and M. Tórtola, *Physics Letters B* **820**, 136508 (2021), arXiv: [2105.08168](#).
- 111 K. N. Abazajian, M. A. Acero, S. K. Agarwalla et al., arXiv e-prints arXiv:1204.5379 (2012), arXiv: [1204.5379](#).
- 112 R. D. Peccei and H. R. Quinn, *Phys. Rev. Lett.***38**, 1440 (1977).
- 113 S. Weinberg, *Phys. Rev. Lett.***40**, 223 (1978).
- 114 F. Wilczek, *Phys. Rev. Lett.***40**, 279 (1978).
- 115 S. Hannestad and T. Schwetz, *J. Cosmology Astropart. Phys.***2016**, 035 (2016), arXiv: [1606.04691](#).
- 116 S. Gariazzo, M. Archidiacono, P. F. de Salas, O. Mena, C. A. Ternes, and M. Tórtola, *J. Cosmology Astropart. Phys.***2018**, 011 (2018), arXiv: [1801.04946](#).
- 117 S. R. Choudhury and S. Hannestad, *J. Cosmology Astropart. Phys.***2020**, 037 (2020), arXiv: [1907.12598](#).
- 118 K. Abazajian, A. Abdughafour, G. E. Addison et al., arXiv e-prints arXiv:2203.08024 (2022), arXiv: [2203.08024](#).
- 119 F. Zwicky, *ApJ***86**, 217 (1937).
- 120 R. A. Flores and J. R. Primack, *ApJ***427**, L1 (1994), arXiv: [astro-ph/9402004](#).
- 121 B. Moore, *Nature***370**, 629 (1994).
- 122 M. Boylan-Kolchin, J. S. Bullock, and M. Kaplinghat, *MNRAS***415**, L40 (2011), arXiv: [1103.0007](#).
- 123 M. R. Buckley and A. H. G. Peter, *Phys. Rep.***761**, 1 (2018), arXiv: [1712.06615](#).
- 124 R. Schaeffer and J. Silk, *ApJ***332**, 1 (1988).
- 125 E. O. Nadler, S. Birrer, D. Gilman et al., *ApJ***917**, 7 (2021), arXiv: [2101.07810](#).
- 126 W. Hu, R. Barkana, and A. Gruzinov, *Phys. Rev. Lett.***85**, 1158 (2000), arXiv: [astro-ph/0003365](#).
- 127 R. Hlozek, D. Grin, D. J. E. Marsh, and P. G. Ferreira, *Phys. Rev. D***91**, 103512 (2015), arXiv: [1410.2896](#).
- 128 D. N. Spergel and P. J. Steinhardt, *Phys. Rev. Lett.***84**, 3760 (2000), arXiv: [astro-ph/9909386](#).

- 129 Z. C. Zeng, A. H. G. Peter, X. Du et al., *MNRAS***513**, 4845 (2022), arXiv: [2110.00259](#).
- 130 S. Hawking, *MNRAS***152**, 75 (1971).
- 131 P. Montero-Camacho, X. Fang, G. Vasquez, M. Silva, and C. M. Hirata, *J. Cosmology Astropart. Phys.***2019**, 031 (2019), arXiv: [1906.05950](#).
- 132 W. Wang, J. Han, M. Cautun, Z. Li, and M. N. Ishigaki, *Science China Physics, Mechanics, and Astronomy* **63**, 109801 (2020), arXiv: [1912.02599](#).
- 133 C.-H. Lin, R. Mandelbaum, M. A. Troxel, C. M. Hirata, and M. Jarvis, *MNRAS***512**, 3312 (2022), arXiv: [2106.10273](#).
- 134 R. E. Sanderson, A. Helmi, and D. W. Hogg, *ApJ***801**, 98 (2015), arXiv: [1404.6534](#).
- 135 P. Salucci, *A&A Rev.***27**, 2 (2019), arXiv: [1811.08843](#).
- 136 A. P. Cooper, S. E. Kuposov, C. Allende Prieto et al., *ApJ***947**, 37 (2023), arXiv: [2208.08514](#).
- 137 M. R. Lovell, V. Eke, C. S. Frenk et al., *MNRAS***420**, 2318 (2012), arXiv: [1104.2929](#).
- 138 K. A. Oman, J. F. Navarro, A. Fattahi et al., *MNRAS***452**, 3650 (2015), arXiv: [1504.01437](#).
- 139 J. Bovy, D. Erkal, and J. L. Sanders, *MNRAS***466**, 628 (2017), arXiv: [1606.03470](#).
- 140 A. Bonaca, D. W. Hogg, A. M. Price-Whelan, and C. Conroy, *ApJ***880**, 38 (2019), arXiv: [1811.03631](#).
- 141 N. Banik, J. Bovy, G. Bertone, D. Erkal, and T. J. L. de Boer, *MNRAS***502**, 2364 (2021), arXiv: [1911.02662](#).
- 142 F. Jiang, A. Benson, P. F. Hopkins et al., *MNRAS***521**, 4630 (2023), arXiv: [2206.12425](#).
- 143 M. Valluri, S. Chabanier, V. Irsic et al., arXiv e-prints arXiv:2203.07491 (2022), arXiv: [2203.07491](#).
- 144 A. Laguë, J. R. Bond, R. Hložek, D. J. E. Marsh, and L. Söding, *MNRAS***504**, 2391 (2021), arXiv: [2004.08482](#).
- 145 N. Palanque-Delabrouille, C. Yèche, N. Schöneberg, J. Lesgourgues, M. Walthar, S. Chabanier, and E. Armengaud, *J. Cosmology Astropart. Phys.***2020**, 038 (2020), arXiv: [1911.09073](#).
- 146 V. Iršič, M. Viel, M. G. Haehnelt et al., *Phys. Rev. D***109**, 043511 (2024), arXiv: [2309.04533](#).
- 147 A. Garzilli, A. Magalich, O. Ruchayskiy, and A. Boyarsky, *MNRAS***502**, 2356 (2021), arXiv: [1912.09397](#).
- 148 E. Puchwein, J. S. Bolton, L. C. Keating et al., *MNRAS***519**, 6162 (2023), arXiv: [2207.13098](#).
- 149 P. Montero-Camacho, C. M. Hirata, P. Martini, and K. Honscheid, *MNRAS***487**, 1047 (2019), arXiv: [1902.02892](#).
- 150 P. Montero-Camacho, Y. Zhang, and Y. Mao, *MNRAS***529**, 3666 (2024), arXiv: [2307.10598](#).
- 151 Euclid Collaboration, R. Scaramella, J. Amiaux et al., *A&A***662**, A112 (2022), arXiv: [2108.01201](#).
- 152 R. Akeson, L. Armus, E. Bachelet et al., arXiv e-prints arXiv:1902.05569 (2019), arXiv: [1902.05569](#).
- 153 H. Aihara, N. Arimoto, R. Armstrong et al., *PASJ***70**, S4 (2018), arXiv: [1704.05858](#).
- 154 H. Aihara, Y. Aisayad, M. Ando et al., *PASJ***74**, 247 (2022), arXiv: [2108.13045](#).
- 155 T. Wang, G. Liu, Z. Cai et al., *Science China Physics, Mechanics, and Astronomy* **66**, 109512 (2023), arXiv: [2306.07590](#).
- 156 N. Benitez, R. Dupke, M. Moles et al., arXiv e-prints arXiv:1403.5237 (2014), arXiv: [1403.5237](#).
- 157 B. Joachimi, R. Mandelbaum, F. B. Abdalla, and S. L. Bridle, *A&A***527**, A26 (2011), arXiv: [1008.3491](#).
- 158 I. Tutusaus, M. Martinelli, V. F. Cardone et al., *A&A***643**, A70 (2020), arXiv: [2005.00055](#).
- 159 J. L. van den Busch, A. H. Wright, H. Hildebrandt et al., *A&A***664**, A170 (2022), arXiv: [2204.02396](#).
- 160 T. Treu, *ARA&A***48**, 87 (2010), arXiv: [1003.5567](#).
- 161 P. Renard, D. Spinoso, P. Montero-Camacho, Z. Sun, H. Zou, and Z. Cai, *MNRAS***535**, 826 (2024), arXiv: [2406.18775](#).
- 162 H. Li, S.-Y. Li, Y. Liu et al., arXiv e-prints arXiv:1710.03047 (2017), arXiv: [1710.03047](#).
- 163 P. Ade, J. Aguirre, Z. Ahmed et al., *J. Cosmology Astropart. Phys.***2019**, 056 (2019), arXiv: [1808.07445](#).
- 164 K. Abazajian, G. Addison, P. Adshead et al., arXiv e-prints arXiv:1907.04473 (2019), arXiv: [1907.04473](#).
- 165 T. Ghigna, A. Adler, K. Aizawa et al., arXiv e-prints arXiv:2406.02724 (2024), arXiv: [2406.02724](#).
- 166 B. M. Sutin, M. Alvarez, N. Battaglia et al., in *Space Telescopes and Instrumentation 2018: Optical, Infrared, and Millimeter Wave*, (edited by M. Lystrup, H. A. MacEwen, G. G. Fazio, N. Batalha, N. Siegler, and E. C. Tong), volume 10698 of *Society of Photo-Optical Instrumentation Engineers (SPIE) Conference Series*, 106984F (2018), arXiv: [1808.01368](#).
- 167 T. Namikawa, A. I. Lonappan, C. Baccigalupi et al., *J. Cosmology Astropart. Phys.***2024**, 010 (2024), arXiv: [2312.05194](#).
- 168 Y.-C. Li, Y.-Z. Ma, M. Remazeilles, and K. Moodley, *Phys. Rev. D***97**, 023514 (2018), arXiv: [1710.10876](#).
- 169 S. R. Furlanetto and A. Lidz, *ApJ***660**, 1030 (2007), arXiv: [astro-ph/0611274](#).
- 170 P. La Plante, J. Mirocha, A. Gorce, A. Lidz, and A. Parsons, *ApJ***944**, 59 (2023), arXiv: [2205.09770](#).
- 171 F. Villaescusa-Navarro, M. Viel, D. Alonso, K. K. Datta, P. Bull, and M. G. Santos, *J. Cosmology Astropart. Phys.***2015**, 034 (2015), arXiv: [1410.7393](#).
- 172 I. P. Carucci, F. Villaescusa-Navarro, and M. Viel, *J. Cosmology Astropart. Phys.***2017**, 001 (2017), arXiv: [1611.07527](#).
- 173 P. Montero-Camacho, C. Morales-Gutiérrez, Y. Zhang, H. Long, and Y. Mao, arXiv e-prints arXiv:2409.11613 (2024), arXiv: [2409.11613](#).
- 174 C. B. V. Dash and T. Guha Sarkar, *J. Cosmology Astropart. Phys.***2021**, 016 (2021), arXiv: [2010.05816](#).
- 175 C. B. V. Dash, T. G. Sarkar, and A. K. Sarkar, *Journal of Astrophysics and Astronomy* **44**, 5 (2023).
- 176 A. K. Sarkar, A. K. Pal, and T. Guha Sarkar, *J. Cosmology Astropart. Phys.***2019**, 058 (2019), arXiv: [1907.10309](#).
- 177 LIGO Scientific Collaboration, J. Aasi, B. P. Abbott et al., *Classical and Quantum Gravity* **32**, 074001 (2015), arXiv: [1411.4547](#).
- 178 P. Amaro-Seoane, H. Audley, S. Babak et al., arXiv e-prints arXiv:1702.00786 (2017), arXiv: [1702.00786](#).
- 179 Z. Luo, Y. Wang, Y. Wu, W. Hu, and G. Jin, *Prog. Theor. Exp. Phys.* **2021** (2021), URL <https://dx.doi.org/10.1093/ptep/ptaa083>.
- 180 M. Punturo, M. Abernathy, F. Acernese et al., *Classical and Quantum Gravity* **27**, 194002 (2010).
- 181 G. Agazie, A. Anumalapudi, A. M. Archibald et al., *ApJ***951**, L8 (2023), arXiv: [2306.16213](#).
- 182 H. Xu, S. Chen, Y. Guo et al., *Research in Astronomy and Astrophysics* **23**, 075024 (2023), arXiv: [2306.16216](#).
- 183 EPTA Collaboration, InPTA Collaboration, J. Antoniadis et al., *A&A***678**, A50 (2023), arXiv: [2306.16214](#).
- 184 CHIME/FRB Collaboration, M. Amiri, B. C. Andersen et al., *ApJS***257**, 59 (2021), arXiv: [2106.04352](#).
- 185 W. Lu and A. L. Piro, *ApJ***883**, 40 (2019), arXiv: [1903.00014](#).
- 186 K. M. Rajwade, M. C. Bezuidenhout, M. Caleb et al., *MNRAS***514**, 1961 (2022), arXiv: [2205.14600](#).
- 187 C.-H. Niu, D. Li, R. Luo et al., *ApJ***909**, L8 (2021), arXiv: [2102.10546](#).
- 188 D. E. Holz and S. A. Hughes, *ApJ***629**, 15 (2005), arXiv: [astro-ph/0504616](#).
- 189 B. P. Abbott, R. Abbott, T. D. Abbott et al., *Nature***551**, 85 (2017), arXiv: [1710.05835](#).
- 190 A. Palmese, O. Graur, J. T. Annis et al., *BAAS***51**, 310 (2019), arXiv: [1903.04730](#).
- 191 C. Cigarrán Díaz and S. Mukherjee, *MNRAS***511**, 2782 (2022), arXiv: [2107.12787](#).

- 192 N. Borghi, M. Mancarella, M. Moresco, M. Tagliuzucchi, F. Iacovelli, A. Cimatti, and M. Maggiore, *ApJ***964**, 191 (2024), arXiv: [2312.05302](#).
- 193 X. P. You, G. Hobbs, W. A. Coles et al., *MNRAS***378**, 493 (2007), arXiv: [astro-ph/0702366](#).
- 194 M. McQuinn, *ApJ***780**, L33 (2014), arXiv: [1309.4451](#).
- 195 Y. Huang, K.-G. Lee, N. I. Libeskind, S. Simha, A. Valade, and J. X. Prochaska, arXiv e-prints arXiv:2410.22098 (2024), arXiv: [2410.22098](#).
- 196 C. W. James, E. M. Ghosh, J. X. Prochaska et al., *MNRAS***516**, 4862 (2022), arXiv: [2208.00819](#).
- 197 S. Hagstotz, R. Reischke, and R. Lilow, *MNRAS***511**, 662 (2022), arXiv: [2104.04538](#).
- 198 A. L. Coil, M. R. Blanton, S. M. Burles et al., *ApJ***741**, 8 (2011), arXiv: [1011.4307](#).
- 199 R. J. Cool, J. Moustakas, M. R. Blanton et al., *ApJ***767**, 118 (2013), arXiv: [1303.2672](#).
- 200 G. B. Brammer, P. G. van Dokkum, M. Franx et al., *ApJS***200**, 13 (2012), arXiv: [1204.2829](#).
- 201 K. Gebhardt, E. Mentuch Cooper, R. Ciardullo et al., *ApJ***923**, 217 (2021), arXiv: [2110.04298](#).
- 202 C. Hahn, M. J. Wilson, O. Ruiz-Macias et al., *AJ***165**, 253 (2023), arXiv: [2208.08512](#).
- 203 R. Zhou, B. Dey, J. A. Newman et al., *AJ***165**, 58 (2023), arXiv: [2208.08515](#).
- 204 A. Raichoor, J. Moustakas, J. A. Newman et al., *AJ***165**, 126 (2023), arXiv: [2208.08513](#).
- 205 E. Chaussidon, C. Yèche, N. Palanque-Delabrouille et al., *ApJ***944**, 107 (2023), arXiv: [2208.08511](#).
- 206 B. Hoyle, K. Paech, M. M. Rau, S. Seitz, and J. Weller, *MNRAS***458**, 4498 (2016), arXiv: [1508.06280](#).
- 207 E. Darragh-Ford, J. F. Wu, Y.-Y. Mao et al., *ApJ***954**, 149 (2023), arXiv: [2212.07433](#).
- 208 S. H. Im, H. S. Hwang, J. Park et al., *ApJ***972**, 196 (2024), arXiv: [2407.18602](#).
- 209 E. M. Hu and R. G. McMahon, *Nature***382**, 231 (1996), arXiv: [astro-ph/9606135](#).
- 210 L. L. Cowie and E. M. Hu, *AJ***115**, 1319 (1998), arXiv: [astro-ph/9801003](#).
- 211 M. White, A. Raichoor, A. Dey et al., *J. Cosmology Astropart. Phys.***2024**, 020 (2024), arXiv: [2406.01803](#).
- 212 M. E. Schwamb, K. Volk, H. Wen et al., arXiv e-prints arXiv:1812.01149 (2018), arXiv: [1812.01149](#).
- 213 A. Dey, D. J. Schlegel, D. Lang et al., *AJ***157**, 168 (2019), arXiv: [1804.08657](#).
- 214 B. Flaugher, H. T. Diehl, K. Honscheid et al., *AJ***150**, 150 (2015), arXiv: [1504.02900](#).
- 215 K.-S. Lee, E. Gawiser, C. Park et al., *ApJ***962**, 36 (2024), arXiv: [2309.10191](#).
- 216 Y. Luo, A. Leauthaud, J. Greene et al., *MNRAS***530**, 4988 (2024), arXiv: [2305.19310](#).
- 217 P. Bull, *MNRAS***471**, 12 (2017), arXiv: [1610.08948](#).
- 218 G. Favole, D. Sapone, and J. Silva Lafaerie, arXiv e-prints arXiv:1912.06155 (2019), arXiv: [1912.06155](#).
- 219 B. Joachimi, C. A. Lin, M. Asgari et al., *A&A***646**, A129 (2021), arXiv: [2007.01844](#).
- 220 J. U. Lange, A. P. Hearin, A. Leauthaud et al., *MNRAS***520**, 5373 (2023), arXiv: [2301.08692](#).
- 221 J. Sohn, M. J. Geller, H. S. Hwang, A. Diaferio, K. J. Rines, and Y. Utsumi, *ApJ***923**, 143 (2021), arXiv: [2106.11429](#).
- 222 J. Sohn, M. J. Geller, H. S. Hwang, D. G. Fabricant, Y. Utsumi, and I. Damjanov, *ApJ***945**, 94 (2023), arXiv: [2210.16499](#).
- 223 DESI Collaboration, A. Aghamousa, J. Aguilar et al., arXiv e-prints arXiv:1611.00036 (2016), arXiv: [1611.00036](#).
- 224 D. J. Heath, *MNRAS***179**, 351 (1977).
- 225 S. Alam, M. Ata, S. Bailey et al., *MNRAS***470**, 2617 (2017), arXiv: [1607.03155](#).
- 226 A. Mainzer, J. Bauer, T. Grav et al., *ApJ***731**, 53 (2011), arXiv: [1102.1996](#).
- 227 A. Raichoor, J. Comparat, T. Delubac et al., *MNRAS***471**, 3955 (2017), arXiv: [1704.00338](#).
- 228 S. Yuan, R. H. Wechsler, Y. Wang et al., arXiv e-prints arXiv:2310.09329 (2023), arXiv: [2310.09329](#).
- 229 H. Gao, Y. P. Jing, K. Xu et al., *ApJ***961**, 74 (2024), arXiv: [2309.03802](#).
- 230 A. E. Shapley, C. C. Steidel, M. Pettini, and K. L. Adelberger, *ApJ***588**, 65 (2003), arXiv: [astro-ph/0301230](#).
- 231 J. M. Le Goff, C. Magneville, E. Rollinde et al., *A&A***534**, A135 (2011), arXiv: [1107.4233](#).
- 232 H. du Mas des Bourboux, J.-M. Le Goff, M. Blomqvist et al., *A&A***608**, A130 (2017), arXiv: [1708.02225](#).
- 233 C. Ravoux, E. Armengaud, M. Walther et al., *J. Cosmology Astropart. Phys.***2020**, 010 (2020), arXiv: [2004.01448](#).
- 234 H. du Mas des Bourboux, J. Rich, A. Font-Ribera et al., *ApJ***901**, 153 (2020), arXiv: [2007.08995](#).
- 235 B. Villassenor, B. Robertson, P. Madau, and E. Schneider, *Phys. Rev. D***108**, 023502 (2023), arXiv: [2209.14220](#).
- 236 L. Fuß and M. Garny, *J. Cosmology Astropart. Phys.***2023**, 020 (2023), arXiv: [2210.06117](#).
- 237 M. J. Wilson and M. White, *J. Cosmology Astropart. Phys.***2019**, 015 (2019), arXiv: [1904.13378](#).
- 238 C. C. Steidel, M. Giavalisco, M. Pettini, M. Dickinson, and K. L. Adelberger, *ApJ***462**, L17 (1996), arXiv: [astro-ph/9602024](#).
- 239 C. C. Steidel, K. L. Adelberger, M. Giavalisco, M. Dickinson, and M. Pettini, *ApJ***519**, 1 (1999), arXiv: [astro-ph/9811399](#).
- 240 N. A. Reddy and C. C. Steidel, *ApJ***692**, 778 (2009), arXiv: [0810.2788](#).
- 241 M. Giavalisco, *ARA&A***40**, 579 (2002).
- 242 Y. Ono, M. Ouchi, Y. Harikane et al., *PASJ***70**, S10 (2018), arXiv: [1704.06004](#).
- 243 N. A. Reddy, C. C. Steidel, M. Pettini, K. L. Adelberger, A. E. Shapley, D. K. Erb, and M. Dickinson, *ApJS***175**, 48 (2008), arXiv: [0706.4091](#).
- 244 H. Hildebrandt, J. Pielorz, T. Erben, L. van Waerbeke, P. Simon, and P. Capak, *A&A***498**, 725 (2009), arXiv: [0903.3951](#).
- 245 J. Cooke, Y. Omori, and E. V. Ryan-Weber, *MNRAS***433**, 2122 (2013), arXiv: [1305.0562](#).
- 246 J. E. Gunn, M. Carr, C. Rockosi et al., *AJ***116**, 3040 (1998), arXiv: [astro-ph/9809085](#).
- 247 J. R. Weaver, O. B. Kauffmann, O. Ilbert et al., *ApJS***258**, 11 (2022), arXiv: [2110.13923](#).
- 248 M. Ouchi, Y. Ono, and T. Shibuya, *ARA&A***58**, 617 (2020), arXiv: [2012.07960](#).
- 249 R. Bacon, J. Brinchmann, S. Conseil et al., *A&A***670**, A4 (2023), arXiv: [2211.08493](#).
- 250 A. Torralba-Torregrosa, S. Gurung-López, P. Arnalte-Mur et al., *A&A***680**, A14 (2023), arXiv: [2307.10215](#).
- 251 A. Torralba-Torregrosa, P. Renard, D. Spinoso et al., *A&A***690**, A388 (2024), arXiv: [2407.19020](#).
- 252 M. Ouchi, Y. Harikane, T. Shibuya et al., *PASJ***70**, S13 (2018), arXiv: [1704.07455](#).
- 253 N. P. Ross, A. D. Myers, E. S. Sheldon et al., *ApJS***199**, 3 (2012), arXiv: [1105.0606](#).
- 254 A. D. Myers, N. Palanque-Delabrouille, A. Prakash et al., *ApJS***221**, 27 (2015), arXiv: [1508.04472](#).
- 255 C. Yèche, N. Palanque-Delabrouille, C.-A. Claveau et al., *Research Notes of the American Astronomical Society* **4**, 179 (2020), arXiv: [2010.11280](#).
- 256 X. Fan, M. A. Strauss, G. T. Richards et al., *AJ***131**, 1203 (2006), arXiv: [astro-ph/0512080](#).

- 257 L. Jiang, X. Fan, J. Annis et al., *AJ***135**, 1057 (2008), arXiv: [0708.2578](#).
- 258 C. J. Willott, P. Delorme, C. Reylé et al., *AJ***139**, 906 (2010), arXiv: [0912.0281](#).
- 259 B. P. Venemans, J. R. Findlay, W. J. Sutherland et al., *ApJ***779**, 24 (2013), arXiv: [1311.3666](#).
- 260 S. L. Reed, R. G. McMahon, M. Banerji et al., *MNRAS***454**, 3952 (2015), arXiv: [1504.03264](#).
- 261 Y. Matsuoka, M. Onoue, N. Kashikawa et al., *ApJ***828**, 26 (2016), arXiv: [1603.02281](#).
- 262 E. Bañados, B. P. Venemans, R. Decarli et al., *ApJS***227**, 11 (2016), arXiv: [1608.03279](#).
- 263 F. Wang, X.-B. Wu, X. Fan et al., *ApJ***819**, 24 (2016), arXiv: [1602.04659](#).
- 264 J. Yang, X.-B. Wu, D. Liu et al., *AJ***155**, 110 (2018), arXiv: [1801.01245](#).
- 265 N. Palanque-Delabrouille, C. Magneville, C. Yèche et al., *A&A***587**, A41 (2016), arXiv: [1509.05607](#).
- 266 C. Yèche, P. Petitjean, J. Rich et al., *A&A***523**, A14 (2010).
- 267 X. Jin, Y. Zhang, J. Zhang, Y. Zhao, X.-b. Wu, and D. Fan, *MNRAS***485**, 4539 (2019), arXiv: [1903.03335](#).
- 268 Planck Collaboration, N. Aghanim, Y. Akrami et al., *A&A***641**, A1 (2020), arXiv: [1807.06205](#).
- 269 C. Radhakrishna Rao, *Bulletin of the Calcutta Mathematical Society* **37**, 81 (1945).
- 270 H. Cramér, *Mathematical Methods of Statistics (PMS-9)*, (Princeton University Press 1946).
- 271 M. Tegmark, *Phys. Rev. Lett.***79**, 3806 (1997), arXiv: [astro-ph/9706198](#).
- 272 W. d'Assignies D, C. Zhao, J. Yu, and J.-P. Kneib, *MNRAS***521**, 3648 (2023), arXiv: [2301.02289](#).
- 273 M. White, Y.-S. Song, and W. J. Percival, *MNRAS***397**, 1348 (2009), arXiv: [0810.1518](#).
- 274 L. Samushia, W. J. Percival, and A. Raccanelli, *MNRAS***420**, 2102 (2012), arXiv: [1102.1014](#).
- 275 B. A. Reid, L. Samushia, M. White et al., *MNRAS***426**, 2719 (2012), arXiv: [1203.6641](#).
- 276 W. J. Percival, D. Burkey, A. Heavens et al., *MNRAS***353**, 1201 (2004), arXiv: [astro-ph/0406513](#).
- 277 L. Guzzo, M. Pierleoni, B. Meneux et al., *Nature***451**, 541 (2008), arXiv: [0802.1944](#).
- 278 S. de la Torre, L. Guzzo, J. A. Peacock et al., *A&A***557**, A54 (2013), arXiv: [1303.2622](#).
- 279 C. Blake, S. Brough, M. Colless et al., *MNRAS***415**, 2876 (2011), arXiv: [1104.2948](#).
- 280 F. Beutler, C. Blake, M. Colless et al., *MNRAS***423**, 3430 (2012), arXiv: [1204.4725](#).
- 281 T. Okumura, C. Hikage, T. Totani et al., *PASJ***68**, 38 (2016), arXiv: [1511.08083](#).
- 282 H. Okada, T. Totani, and S. Tsujikawa, *Phys. Rev. D***87**, 103002 (2013), arXiv: [1208.4681](#).
- 283 A. De Felice and S. Tsujikawa, *J. Cosmology Astropart. Phys.***2012**, 007 (2012), arXiv: [1110.3878](#).
- 284 T. Baker, P. Ferreira, and C. Skordis, *Phys. Rev. D***89**, 024026 (2014), arXiv: [1310.1086](#).
- 285 W. Hu and I. Sawicki, *Phys. Rev. D***76**, 064004 (2007), arXiv: [0705.1158](#).
- 286 V. Desjacques, D. Jeong, and F. Schmidt, *Physics Reports* **733**, 1 (2018).
- 287 T. Lazeyras, A. Barreira, F. Schmidt, and V. Desjacques, *J. Cosmology Astropart. Phys.***2023**, 023 (2023), arXiv: [2209.07251](#).
- 288 A. Gutiérrez Adame, S. Avila, V. Gonzalez-Perez et al., *PNG-UNITsims: Halo clustering response to primordial non-Gaussianities as a function of mass (2024)*, arXiv: [2312.12405](#).
- 289 J. M. Sullivan, T. Pijon, and U. Seljak, *J. Cosmology Astropart. Phys.***2023**, 004 (2023), arXiv: [2303.08901](#).
- 290 S. Ferraro and M. J. Wilson, *BAAS***51**, 72 (2019), arXiv: [1903.09208](#).
- 291 A. Ghoshal and A. Naskar, *European Physical Journal C* **84**, 999 (2024), arXiv: [2302.00668](#).
- 292 A. J. Ross, W. J. Percival, A. Carnero et al., *MNRAS***428**, 1116 (2013).
- 293 M. Tristram, A. J. Banday, M. Douspis et al., *A&A***682**, A37 (2024), arXiv: [2309.10034](#).
- 294 A. Arinyo-i-Prats, J. Miralda-Escudé, M. Viel, and R. Cen, *J. Cosmology Astropart. Phys.***2015**, 017 (2015), arXiv: [1506.04519](#).
- 295 D. Foreman-Mackey, D. W. Hogg, D. Lang, and J. Goodman, *PASP***125**, 306 (2013), arXiv: [1202.3665](#).
- 296 P. Montero-Camacho and Y. Mao, *MNRAS***508**, 1262 (2021), arXiv: [2106.14492](#).
- 297 A. Font-Ribera, P. McDonald, N. Mostek, B. A. Reid, H.-J. Seo, and A. Slosar, *J. Cosmology Astropart. Phys.***2014**, 023 (2014), arXiv: [1308.4164](#).
- 298 N. Banik, J. Bovy, G. Bertone, D. Erkal, and T. J. L. de Boer, *J. Cosmology Astropart. Phys.***2021**, 043 (2021), arXiv: [1911.02663](#).
- 299 A. Dekker, S. Ando, C. A. Correa, and K. C. Y. Ng, *Phys. Rev. D***106**, 123026 (2022), arXiv: [2111.13137](#).
- 300 E. O. Nadler, A. Drlica-Wagner, K. Bechtol et al., *Phys. Rev. Lett.***126**, 091101 (2021), arXiv: [2008.00022](#).
- 301 R. E. Keeley, A. M. Nierenberg, D. Gilman et al., arXiv e-prints arXiv:2405.01620 (2024), arXiv: [2405.01620](#).